

Hedgehog signaling from the ZPA, through FMN1 and Gremlin [Duijf et al., 2003]. FMN1, which represses BMP signaling in association with cytoskeleton components, has previously been implicated in limb development [Zhou et al., 2009]. SMOC1 also functions as a BMP antagonist in early embryogenesis, which provides a plausible explanation for both the limb and eye phenotype in humans and mice [Okada et al., 2011; Rainger et al., 2011].

In conclusion, *FNBP4* is mutated in a Lebanese family with MLA. This knowledge is useful to understand development of eye and limb in humans.

## ACKNOWLEDGMENTS

We would like to thank the patients and their families for their participation in this study. This work was supported by the Ministry of Health, Labor and Welfare of Japan, a Grant-in-Aid from the Japan Society for the Promotion of Science, a Grant-in-Aid for Young Scientists from the Japan Society for the Promotion of Science, the Japan Science and Technology Agency, the Strategic Research Program for Brain Sciences, a Grant-in-Aid for Scientific Research on Innovative Areas (Transcription Cycle) from the Ministry of Education, Culture, Sports, Science and Technology of Japan and Takeda Science Foundation.

## REFERENCES

- Abouzeid H, Boisset G, Favez T, Youssef M, Marzouk I, Shakankiry N, Bayoumi N, Descombes P, Agosti C, Munier FL, Schorderet DF. 2011. Mutations in the SPARC-related modular calcium-binding protein 1 gene, SMOC1, cause waardenburg anophthalmia syndrome. *Am J Hum Genet* 88:92–98.
- Bahlo M, Bromhead CJ. 2009. Generating linkage mapping files from Affymetrix SNP chip data. *Bioinformatics* 25:1961–1962.
- Duijf PH, van Bokhoven H, Brunner HG. 2003. Pathogenesis of split-hand/split-foot malformation. *Hum Mol Genet* 12:R51–R60.
- Frazier JA, Field CM. 1997. Actin cytoskeleton: Are FH proteins local organizers? *Curr Biol* 7:R414–R417.
- Garavelli L, Pedori S, Dal Zotto R, Franchi F, Marinelli M, Croci GF, Bellato S, Ammenti A, Virdis R, Banchini G, Superti-Furga A. 2006. Anophthalmos with limb anomalies (Waardenburg ophthalmos (sic)-acromelic syndrome): report of a new Italian case with renal anomaly and review. *Genet Couns* 17:449–455.
- Hamanoue H, Megarbane A, Tohma T, Nishimura A, Mizuguchi T, Saitsu H, Sakai H, Miura S, Toda T, Miyake N, Niikawa N, Yoshiura K, Hirahara F, Matsumoto N. 2009. A locus for ophthalmos-acromelic syndrome mapped to 10p11.23. *Am J Med Genet Part A* 149A:336–342.
- Megarbane A, Souraty N, Tamraz J. 1998. Ophthalmos-acromelic syndrome (Waardenburg) with split hand and polydactyly. *Genet Couns* 9:195–199.
- Okada I, Hamanoue H, Terada K, Tohma T, Megarbane A, Chouery E, Abou-Ghoch J, Jalkh N, Cogulu O, Ozkinay F, Horie K, Takeda J, Furuichi T, Ikegawa S, Nishiyama K, Miyatake S, Nishimura A, Mizuguchi T, Niikawa N, Hirahara F, Kaname T, Yoshiura K, Tsurusaki Y, Doi H, Miyake N, Furukawa T, Matsumoto N, Saitsu H. 2011. SMOC1 is essential for ocular and limb development in humans and mice. *Am J Hum Genet* 88:30–41.
- Rainger J, van Beusekom E, Ramsay JK, McKie L, Al-Gazali L, Pallotta R, Saponari A, Branney P, Fisher M, Morrison H, Bicknell L, Gautier P, Perry P, Sokhi K, Sexton D, Bardakjian TM, Schneider AS, Elcioglu N, Ozkinay F, Koenig R, Megarbane A, Semerci CN, Khan A, Zafar S, Hennekam R, Sousa SB, Ramos L, Garavelli L, Furga AS, Wischmeijer A, Jackson IJ, Gillissen-Kaesbach G, Brunner HG, Wieczorek D, van Bokhoven H, Fitzpatrick DR. 2011. Loss of the BMP antagonist, SMOC-1, causes Ophthalmos-acromelic (Waardenburg Anophthalmia) syndrome in humans and mice. *PLoS Genet* 7:e1002114.
- Robledo RF, Rajan L, Li X, Lufkin T. 2002. The Dlx5 and Dlx6 homeobox genes are essential for craniofacial, axial, and appendicular skeletal development. *Genes Dev* 16:1089–1101.
- Wasserman S. 1998. FH proteins as cytoskeletal organizers. *Trends Cell Biol* 8:111–115.
- Zhou F, Leder P, Zuniga A, Dettenhofer M. 2009. Formin1 disruption confers oligodactylism and alters Bmp signaling. *Hum Mol Genet* 18:2472–2482.

## Mitochondrial Complex III Deficiency Caused by a Homozygous *UQCRC2* Mutation Presenting with Neonatal-Onset Recurrent Metabolic Decompensation

Noriko Miyake,<sup>1\*†</sup> Shoji Yano,<sup>2†</sup> Chika Sakai,<sup>3</sup> Hideyuki Hatakeyama,<sup>3</sup> Yuichi Matsushima,<sup>3</sup> Masaaki Shiina,<sup>4</sup> Yoriko Watanabe,<sup>5</sup> James Bartley,<sup>6</sup> Jose E. Abdenur,<sup>7</sup> Raymond Y. Wang,<sup>7</sup> Richard Chang,<sup>7</sup> Yoshinori Tsurusaki,<sup>1</sup> Hiroshi Doi,<sup>1</sup> Mitsuko Nakashima,<sup>1</sup> Hiroto Saito,<sup>1</sup> Kazuhiro Ogata,<sup>4</sup> Yu-ichi Goto,<sup>3</sup> and Naomichi Matsumoto<sup>1\*</sup>

<sup>1</sup>Department of Human Genetics, Yokohama City University Graduate School of Medicine, Yokohama, Japan; <sup>2</sup>Genetics Division, Department of Pediatrics, LAC + USC Medical Center, Keck School of Medicine, University of Southern California, Los Angeles, California; <sup>3</sup>Department of Mental Retardation and Birth Defect Research, National Institute of Neuroscience, NCNP, Kodaira, Tokyo, Japan; <sup>4</sup>Department of Biochemistry, Yokohama City University Graduate School of Medicine, Yokohama, Japan; <sup>5</sup>Department of Pediatrics and Child Health, Kurume University School of Medicine, Kurume, Japan; <sup>6</sup>Division of Medical Genetics, Department of Pediatrics, Children's Hospital Los Angeles, Los Angeles, California; <sup>7</sup>Division of Metabolic Disorders, CHOC Children's, Orange, California

Communicated by Daniel Nebert

Received 26 June 2012; accepted revised manuscript 7 November 2012.

Published online 19 December 2012 in Wiley Online Library (www.wiley.com/humanmutation). DOI: 10.1002/humu.22257

**ABSTRACT:** Mitochondrial complex III (CIII) deficiency is a relatively rare disease with high clinical and genetic heterogeneity. CIII comprises 11 subunits encoded by one mitochondrial and 10 nuclear genes. Abnormalities of the nuclear genes such as *BCS1L* and *TTC19* encoding mitochondrial assembly factors are well known, but an explanation of the majority of CIII deficiency remains elusive. Here, we report three patients from a consanguineous Mexican family presenting with neonatal onset of hypoglycemia, lactic acidosis, ketosis, and hyperammonemia. We found a homozygous missense mutation in *UQCRC2* that encodes mitochondrial ubiquinol-cytochrome *c* reductase core protein II by whole-exome sequencing combined with linkage analysis. On the basis of structural modeling, the mutation (p.Arg183Trp) was predicted to destabilize the hydrophobic core at the subunit interface of the core protein II homodimer. *In vitro* studies using fibroblasts from the index patient clearly indicated CIII deficiency, as well as impaired assembly of the supercomplex formed from complexes I, III, and IV. This is the

first described human disease caused by a core protein abnormality in mitochondrial CIII.

Hum Mutat 34:446–452, 2013. © 2012 Wiley Periodicals, Inc.

**KEY WORDS:** mitochondrial complex III (CIII); *UQCRC2*; whole exome sequence; supercomplex

### Introduction

The mitochondrial respiratory chain generates energy as ATP by means of the electron-transport chain and the oxidative-phosphorylation system. The mitochondrial respiratory chain, located in the inner mitochondrial membrane, is composed of five multimeric protein complexes: I, II, III, IV, and V. Among them, the complex III (CIII) (bc<sub>1</sub> complex or ubiquinol-cytochrome *c* reductase; EC1.10.2.2) monomer is composed of 11 proteins [Iwata et al., 1998]. One protein is encoded by mitochondrial DNA (*MTCYB*) and the other 10 are encoded by nuclear DNA. The latter are categorized into three groups: (1) core proteins (encoded by *UQCRC1* and *UQCRC2*), (2) respiratory proteins (*CYC1* and *UQCRFS1*), and (3) low-molecular-weight proteins (*UQCRH*, *UQCRB*, *UQCRCQ*, *UCRC*, *UQCRI1*, and *UQCRFS1*). In its native state, the CIII monomer is quickly converted into a catalytically active homodimer that is incorporated into a supercomplex (respirasome) with complexes I and IV, and this supercomplex functions as a single enzyme [Schagger and Pfeiffer, 2000].

Mitochondrial CIII enzyme deficiency (CIII deficiency; MIM# 124000) is a relatively rare disease with clinical and genetic heterogeneity. Until now, mutations in four genes have been known to cause autosomal recessive CIII deficiencies: *UQCRB* (NM\_006294), *UQCRCQ* (NM\_014402), *BCS1L* (NM\_004328), and *TTC19* (NM\_017775). *UQCRB* and *UQCRCQ* encode components of CIII itself, whereas *BCS1L* and *TTC19* produce mitochondrial assembly factors. Although recessive *BCS1L* mutations are the most frequent cause of CIII deficiency, the majority of the genetic causes of CIII deficiency remain unknown [Benit et al., 2009; de Lonlay et al.,

Additional Supporting Information may be found in the online version of this article.

<sup>†</sup>These authors contributed equally to this work.

\*Correspondence to: Noriko Miyake, Department of Human Genetics, Yokohama City University Graduate School of Medicine, 3-9 Fukuura, Kanazawa-ku, Yokohama 236-0004, Japan. E-mail: Noriko Miyake: nmiyake@yokohama-cu.ac.jp; or Naomichi Matsumoto, Department of Human Genetics, Yokohama City University Graduate School of Medicine, 3-9 Fukuura, Kanazawa-ku, Yokohama 236-0004, Japan. E-mail: naomat@yokohama-cu.ac.jp

Contract grant sponsors: Ministry of Health, Labor, and Welfare; the Japan Science and Technology Agency; the Strategic Research Program for Brain Sciences; Ministry of Education, Culture, Sports, Science, and Technology of Japan; the Japan Society for the Promotion of Science; 2011 Strategic Research Promotion of Yokohama City University; the Japan Epilepsy Research Foundation; and the Takeda Science Foundation.

2001; DiMauro and Schon, 2003; Fernandez-Vizarra et al., 2007; Hinson et al., 2007; Visapaa et al., 2002]. Interestingly, *BCS1L* mutations cause variable clinical presentations: Bjornstad syndrome (MIM# 262000), which is characterized by sensorineural hearing loss and pili torti [Hinson et al., 2007]; GRACILE syndrome (MIM# 603358), which presents with fetal growth retardation, aminoaciduria, cholestasis, iron overload, lactic acidosis, and early death [Visapaa et al., 2002]; and Leigh syndrome (MIM# 256000) [de Lonlay et al., 2001]. A homozygous mutation of *TTC19* causes a progressive neurodegenerative disorder [Ghezzi et al., 2011]. A homozygous 4-bp deletion of *UQCRB* causes hypoglycemia and lactic acidosis [Haut et al., 2003] and a homozygous missense mutation of *UQCRQ* results in severe psychomotor retardation, extrapyramidal signs, and dementia [Barel et al., 2008].

Here, we describe the first human mutation of *UQCRC2* encoding core protein 2 of CIII, utilizing linkage analysis and whole-exome sequencing.

## Materials and Methods

### DNA Preparation

DNAs from family members and fibroblasts from patients were collected after obtaining informed consent. DNA was extracted from blood leukocytes using a QIAamp DNA Blood Midi Kit (Qiagen, Hilden, Germany) or QuickGene-610L (Fujifilm, Tokyo, Japan), according to the manufacturers' instructions. DNAs from 80 Mexican control subjects were purchased from the Coriell Institute for Medical Research (Camden, New Jersey). The experimental protocols were approved by the institutional review board of Yokohama City University.

### Linkage Analysis

SNP typing was performed using an Affymetrix Human Mapping SNP 10K Xba I 142 2.0 array (Affymetrix, Santa Clara, California), according to the manufacturer's instructions. A multipoint linkage analysis was performed using Allegro version 2.0 [Gudbjartsson et al., 2005]. An autosomal recessive mode of inheritance with complete penetrance and a disease allele frequency of 0.005 was used.

### Exome Sequence

Briefly, 3  $\mu$ g of genomic DNA was sheared and captured using a NimbleGen SeqCap EZ Exome Library SR (Roche NimbleGen, Inc., Madison, New Jersey), according to the manufacturer's instructions. The captured sample was sequenced on a GAIIX instrument (Illumina, Inc., San Diego, California) using 76-bp paired-end reads. Image analysis and base calling were performed by sequence-control software real-time analysis (Illumina, Inc.) and CASAVA software v1.7 (Illumina, Inc.). The quality-controlled (path-filtered) reads were mapped to human genome reference hg19 with Mapping and Assembly with Qualities (MAQ; <http://maq.sourceforge.net/>) and NextGENe software v2.00 (SoftGenetics, State College, Pennsylvania). The variants from MAQ were annotated by SeattleSeq annotation 131 (<http://snp.gs.washington.edu/SeattleSeqAnnotation131>). The priority scheme of the variants was described previously [Tsurusaki et al., 2011]. The nucleotide numbering of the variants reflects the cDNA numbering, with +1 corresponding to the A of the ATG translation initiation codon in the reference sequence, accord-

ing to journal guidelines ([www.hgvs.org/mutnomen](http://www.hgvs.org/mutnomen)). The initiation codon is codon 1.

### Expression Vector Preparation

For construction of a mammalian expression vector, full-length *UQCRC2* (NM\_003366.2) was amplified from a cDNA library from a multiple-tissue cDNA (MTC) panel (Clontech, Mountain View, California) using KOD-plus DNA polymerase (Toyobo, Osaka, Japan). The PCR product was cloned into the entry vector (pDONR<sup>TM</sup>221) of the gateway system (Invitrogen, Carlsbad, California). Each of the two missense mutations was independently introduced into the entry clone using a QuickChange II XL site-directed mutagenesis kit (Stratagene, La Jolla, California). Each insert was cloned into pcDNA-DEST40 (C-terminal V5 and 6xHis tag) by LR recombination. All the clones were verified by direct sequencing. In addition, full-length *UQCRC2* (wild type, mutant, or SNP [rs4850: c.548G>A, p.Arg183Gln]) and AcGFP constructs were cloned into multiple cloning sites A and B of the pIRES vector (Clontech).

### Intracellular Localization

Each mammalian expression construct (200 ng) was transfected into COS-1 cells using FuGENE6 (Roche Diagnostics, Indianapolis, Indiana). After 24 hr of transfection, MitoTracker Red CMXRos (Invitrogen) was added and incubated for 30 min. The cells were then fixed with 4% paraformaldehyde for 20 min at room temperature. After permeabilization with 0.1% Triton/1  $\times$  PBS for 10 min, C-terminally V5-6xHis-tagged *UQCRC2* protein was stained with a mouse anti-V5 antibody (1:1,000) (Invitrogen) and an Alexa Fluor 488-conjugated goat antimouse IgG secondary antibody (1:1,000) (Molecular Probes, Carlsbad, California). Confocal images were taken with a FLUOVIEW FV1000-D microscope (Olympus, Tokyo, Japan).

### Mitochondrial Enzyme Activity Assay

Mitochondrial enzyme activities were measured using a previously reported method [Trounce et al., 1996], with slight modifications. The complex I activity is indicated as the rotenone-sensitive NADH-CoQ1 reductase activity. In control assays, the activity was decreased to 20% by rotenone.

### Western Blotting

Mitochondrial enzyme activity and supercomplex formation were analyzed by western blotting. The enzyme activities of the mitochondrial respiratory chain complexes were measured using mitochondrial fractions prepared from primary fibroblasts derived from patient 1 ( $n = 3$ ) and control subjects ( $n = 10$ ). Each measurement was basically performed in triplicate (if the available materials allowed). The values were normalized to complex II or citrate synthase. Immunoblot detection of each respiratory chain complex was performed using mitochondria solubilized with 0.5% *n*-dodecyl- $\beta$ -D-maltoside (DDM). The same amount of pooled mitochondrial protein from control subjects ( $n = 10$ ) was used as the control. The primary antibodies used were as follows: 2  $\mu$ g/ml anti-NDUFA9 (complex I; Invitrogen), 0.02  $\mu$ g/ml anti-SDHA (complex II; Invitrogen), 2  $\mu$ g/ml anti-UQCRC1 (CIII; Abcam, Cambridge, Massachusetts), 0.2  $\mu$ g/ml anti-MTCO1 (complex IV; Invitrogen), and

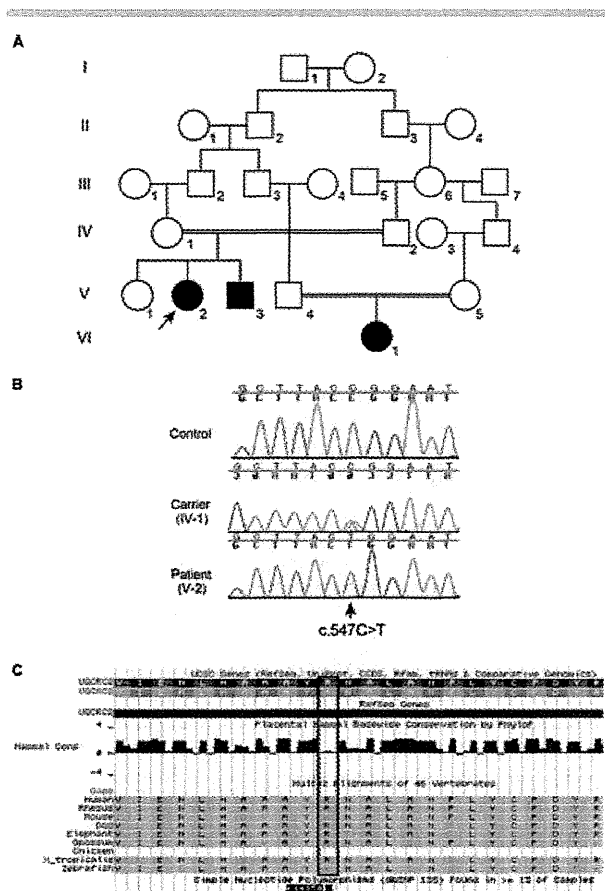


**Figure 1.** Identification of a *UQCRC2* mutation in a consanguineous Mexican family. **A:** Pedigree of the reported family. The arrow indicates the proband. **B:** Electropherogram of the c.547C>T *UQCRC2* mutation. All three patients (1, 2, and 3) showed a homozygous change, whereas the parents and an unaffected sibling of patients 1 and 2 were heterozygous carriers. The arrow indicates c.547C>T. **C:** Evolutionary conservation of p.Arg183 in *UQCRC2* outlined in red. rs4850 (chr 16: 21976762, G>A, p.Arg183Gln) is a common SNP based on the dbSNP135 database.

2  $\mu\text{g/ml}$  anti-ATP5B (complex V; Invitrogen). Immunoblot detection of the respiratory supercomplex was performed using mitochondria solubilized with 1% (w/v) digitonin. The same amount of pooled mitochondrial protein from control subjects ( $n = 10$ ) was used as the control. The primary antibodies used were as follows: 0.02  $\mu\text{g/ml}$  anti-SDHA (complex II; Invitrogen) and 2  $\mu\text{g/ml}$  anti-UQCRC1 (CIII; Abcam). The band intensity of the supercomplex was estimated by densitometry and normalized to that of complex II. The data were obtained by three independent assays.

## Results

Patient 1 (V:2 in Fig. 1A) is a Hispanic female born to a 26-year-old healthy female (G2P2Ab0) and a 28-year-old healthy male who are second cousins. She was delivered at 37 weeks by Cesarean section because of a pathological cardiotocogram. At birth, she weighed 2,329 g (5–10th percentile) with a length of 46 cm (5–10th percentile), and her occipitofrontal circumference was 34 cm (25–50th percentile). Her Apgar scores were 8, 9, and 9 at 1, 5, and 10 min, respectively. She developed a severe metabolic acidosis

(pH 7.1, with a base excess of  $-24.6$  mEq/l) within 1 day, requiring admission to a neonatal intensive care unit. Blood lactate and pyruvate on admission were 25.5 mM (reference range:  $<2.2$  mM) and 0.436 mM (reference range:  $<0.16$  mM), respectively (lactate to pyruvate ratio = 58.48). Clinical examination revealed tachypnea (47 breaths/min), tachycardia (181 beats/min), mild subcostal retractions, Levine II/VI systolic cardiac murmur, no organomegaly, and poor sucking reflex. Blood ammonia was 126  $\mu\text{M}$  (reference range in neonates:  $<80$   $\mu\text{M}$ ). The patient responded promptly to supportive therapy, with intravenous glucose infusion providing 10 mg/kg/min and a sodium bicarbonate drip improving the blood lactate level down to 12.7 mM within 24 hr. The lactate and pyruvate levels further improved to 3.1 and 0.125 mM within 3 days, respectively. Urine organic acid analysis on admission was remarkable for massive lactic and pyruvic aciduria, as well as ketonuria. Plasma amino acids were remarkable for a high alanine level (1,519  $\mu\text{M}$ ; reference range: 200–600  $\mu\text{M}$ ). Magnetic resonance imaging (MRI) of the brain revealed small right parietal and temporal infarcts.

She recovered without sequelae and was discharged on full oral feeds with a high-carbohydrate, reduced-fat formula (60% of calories from carbohydrate, 30% of calories from fat) after 1.5 months of hospitalization. She was also diagnosed with an atrial septal defect and renal tubular acidosis. After the initial hospitalization, she was hospitalized more than 10 times because of episodic metabolic decompensation with lactic acidosis (highest value was 10.8 mM at the age of 3 years and 10 months), hyperammonemia (highest value was 346  $\mu\text{M}$  at the age of 3 years and 3 months), ketosis, and hypoglycemia, which were triggered by intercurrent illnesses including fevers, vomiting, and diarrhea. The patient is now 5 years of age, with normal growth and no signs of intellectual disability. The frequency of hospitalization has decreased, although she still requires urgent medical treatment with intravenous glucose infusion to prevent metabolic decompensation during intercurrent illnesses.

Patient 2 (V:3 in Fig. 1A) is a younger full sibling of patient 1. He was born at 39 weeks of gestation by repeat Cesarean section. At birth, he weighed 2,658 g (5–10th percentile) with a length of 49 cm (25–50th percentile), and his occipitofrontal circumference was 34.3 cm (25th percentile). His Apgar scores were 8 and 9 at 1 and 5 min, respectively. He developed tachypnea, grunting, and poor feeding within 1 day because of lactic acidemia. The initial capillary blood gas showed a pH of 7.05,  $p\text{CO}_2$  of 25 mmHg, bicarbonate of 5.8 mmol/l, and a base excess of  $-22$  mEq/l. He was intubated for 2 days and treated with intravenous glucose infusion and a bicarbonate drip to correct the metabolic acidosis. Feeding with a high-carbohydrate, reduced-fat formula was started in 10 days. His initial hospitalization was 1-month long, during which he was diagnosed with congenital lactic acidemia and persistent hypoglycemia of unknown etiology. He was treated with corticosteroid replacement therapy owing to adrenal insufficiency for 4 months until a normal adrenocorticotropic hormone stimulation test was obtained. At the age of 8 months, he was found unresponsive after 6 hr of fasting owing to decreased appetite associated with a 2-day mild upper-respiratory-tract infection. At a local emergency room, metabolic acidosis (pH 7.23), hypoglycemia (3 mg/dl; reference range:  $>60$  mg/dl), and hyperammonemia (463  $\mu\text{M}$ ), as well as ketosis (blood and urine), were noted. He had five episodes of generalized seizure associated with this episode. Following treatment with levetiracetam, he has been seizure free. Brain MRI findings at the age of 8 months were unremarkable. He was hospitalized for 1 month and discharged without sequelae, and had more than 10 hospitalizations because of similar episodes of lactic acidosis, hypoglycemia, hyperammonemia, and ketosis triggered by intercurrent illnesses. Developmental delay was noted once at 4 months of age. Following

physical and speech therapy, his development was later evaluated as normal at 3 years of age. He is now 4 years of age, with normal growth and no signs of intellectual disability. Physical examination revealed neither dysmorphic features nor abnormal focal neurological signs. He has been fed with a reduced-fat, high-carbohydrate diet and fasting precautions. The frequency of hospitalization has decreased, although he continues to require urgent medical treatment with intravenous glucose infusion to prevent metabolic decompensation during intercurrent illnesses. Laboratory study data obtained in the acute severe metabolic decompensation stage at 16 months of age were remarkable, which are as follows: pH 7.19 capillary blood gas, 11 mg/dl glucose, 348  $\mu$ M blood ammonia, and 6.8 mM blood lactate. Urine organic acid analysis showed markedly elevated 3-hydroxybutyrate and acetoacetate indicating severe ketosis, markedly elevated lactate and pyruvate indicating lactic acidosis, markedly elevated dicarboxylic acids (adipic acid, 1,194 mmol/mol Cr [reference range: <15 mmol/mol Cr], suberic acid, 122 mmol/mol Cr [reference range: <7 mmol/mol Cr], sebacic acid, 288 mmol/mol Cr [reference range: <2 mmol/mol Cr]) indicating hyperactive fatty acid beta oxidation, and moderately elevated tricarboxylic acid cycle intermediates including malate, fumarate, and 2-oxoglutarate. Plasma amino acids showed elevated alanine at 440  $\mu$ M (reference range: 23–410  $\mu$ M). Acylcarnitine profiles obtained at 19 months of age in mild decompensation showed marked elevation of C2 (48 nmol/ml [reference range: 2.6–15.5 nmol/ml]) and moderate elevation of 3-hydroxyacylcarnitines (C12–C18).

Patient 3 (VI:1 in Fig. 1A) is a girl born to consanguineous parents within the same pedigree as patients 1 and 2, but in a different branch. She was small for gestational age and was born vaginally to a 23-year-old mother after a full-term gestation. Her birth weight was 2,200 g. Initially, she had mild respiratory distress and required 1 additional day of monitoring. By 18 months of age, she had undergone four hospitalizations for vomiting, dehydration, and hypoglycemia. An initial blood examination at 18 months of age showed that her blood glucose was 17 mg/dl, bicarbonate was 8 mmol/l, and anion gap was 30 mmol/l. The simultaneous blood lactate and pyruvate levels were 26.3 mg/dl (reference range: <16.0 mg/dl) and 1.5 mg/dl (reference range: <1.5 mg/dl), respectively. She responded quickly to intravenous dextrose with correction of the hypoglycemia and metabolic acidosis. She had developmental delay and microcephaly (second percentile) that led to a brain MRI, but this was interpreted as normal. At 18 months, she spoke only two words but could follow two-part commands. She walked at 15 months of age and had low body weight until starting occupational therapy at 14 months of age. She was not dysmorphic. Her muscle strength and tone were normal when she was in good health, allowing her to climb, hop, and jump in a manner appropriate for her age.

Considering the consanguinity in this family, we hypothesized that the disease was inherited in an autosomal recessive fashion. Linkage analysis using two patients (1 and 2) and three unaffected family members (IV:1, IV:2, and V:1) indicated that homozygous regions totaling 36-Mb were shared by the two affected individuals with logarithm of the odds scores  $\geq 2.0$ , as calculated by Allegro version 2 [Gudbjartsson et al., 2005] (Supp. Table S1). We then performed whole-exome sequencing of DNA from patient 1. Two homozygous variants within the 36-Mb homozygous regions were identified: c.547C>T, p.Arg183Trp in *UQCRC2* (NM\_003366) and c.1675A>G, p.Met559Val in *TNRC6A* (NM\_014494). Sanger sequencing confirmed the two variants in patient 1. The Polyphen-2 program (<http://genetics.bwh.harvard.edu/pph2/>) predicted that p.Arg183Trp in *UQCRC2* and p.Met559Val in *TNRC6A* were probably damaging and benign, respectively (Table 1). *TNRC6A* was

**Table 1. Prediction of Mutational Effects in UQCRC2**

Mutation	Alteration	Type	Grantham score <sup>a</sup>	Polyphen-2	Energy ddG <sup>b</sup>
c.547C>T	p.Arg183Trp	Mutant	101	0.998	10.02
c.548G>A	p.Arg183Gln	SNP	43	0.177	2.19
c.547_548CG>AA	p.Arg183Lys	Ortholog	26	0.001	1.74

<sup>a</sup>Grantham score indicates the chemical dissimilarity caused by codon replacements.

<sup>b</sup>The corrected average interaction energy ddG of each altered amino acid is calculated by FoldX as homozygous mutation.

ruled out as a candidate because the heterozygous *TNRC6A* change was found in patient 3. *UQCRC2* encodes ubiquinol–cytochrome c reductase core protein II (*UQCRC2*; MIM# 191329), a core protein of CIII. All three patients possessed the homozygous p.Arg183Trp change in *UQCRC2*, whereas the father (IV-2), mother (IV-1), and sister (V-1) (all unaffected) were heterozygous (Fig. 1B). This change was not observed among 80 Mexican control alleles or 750 Japanese control alleles.

To predict the effect of the missense mutation (c.547C>T, p.Arg183Trp) on the structural stability of CIII, we calculated the free-energy change of interactions between the core protein monomers (encoded by *UQCRC2*) with and without the mutation using FoldX software (version 3.0) [Guerois et al., 2002; Khan and Vihinen, 2010]. For this calculation, we used the crystal structure of bovine CIII (PDB code 2A06) as a structural model because no crystal structure is available for human *UQCRC2*. Amino acid position 183 of *UQCRC2* is a highly conserved basic amino acid among species from zebrafish to humans (e.g., Arg in humans and cows, Lys in mice; Fig. 1C) and is reported to be substituted for Gln as a nonsynonymous human SNP (rs4850 [c.548G>A, p.Arg183Gln]) (Fig. 1C). Therefore, we also calculated the interaction-energy change upon replacement of Arg183 with Lys or Gln, in addition to the Trp found in the patient. The calculated interaction-energy change caused by replacement of Arg183 with Trp was estimated as 10 kcal/mol, whereas those caused by replacement with Lys or Gln were no more than 2 kcal/mol (Fig. 2A, Table 1). The molecular structure of the wild-type core protein homodimer indicated that the methylene part of the Arg183 side chain of one subunit forms a hydrophobic core with the side chains of His254 and Phe449 of the other subunit at the homodimer interface (Fig. 2B and C). When the Arg183 of the core protein was replaced by Trp, the introduced Trp183 side chain flipped outward from the original side-chain position because of steric hindrance (Fig. 2D). In contrast, when Arg183 was replaced by Lys or Gln, each side chain occupied the original position to maintain a hydrophobic core with the methylene part of Lys or Gln (Fig. 2E and F). This indicates that the Arg183Trp mutation in *UQCRC2* would disrupt the hydrophobic core formed at the interface of the *UQCRC2*-containing complex, resulting in destabilization of CIII. In vitro experiments showing that the exogenous and endogenous expressions of the *UQCRC2* mutant were significantly reduced (Supp. Figs. S1 and S2) may support the protein instability.

To test whether this mutation alters *UQCRC2* localization at the mitochondrial inner membrane, we created mammalian full-length wild-type, mutant, and SNP (rs4850) constructs; transiently overexpressed them in COS1 cells; and observed their localization microscopically. The mutant protein colocalized with mitochondria, similar to the wild-type and SNP proteins (Supp. Fig. S3). This indicates that the p.Arg183Trp mutation probably does not alter the intracellular localization.

To evaluate mitochondrial function in vitro, we measured the enzyme activities of the mitochondrial respiratory chain complexes

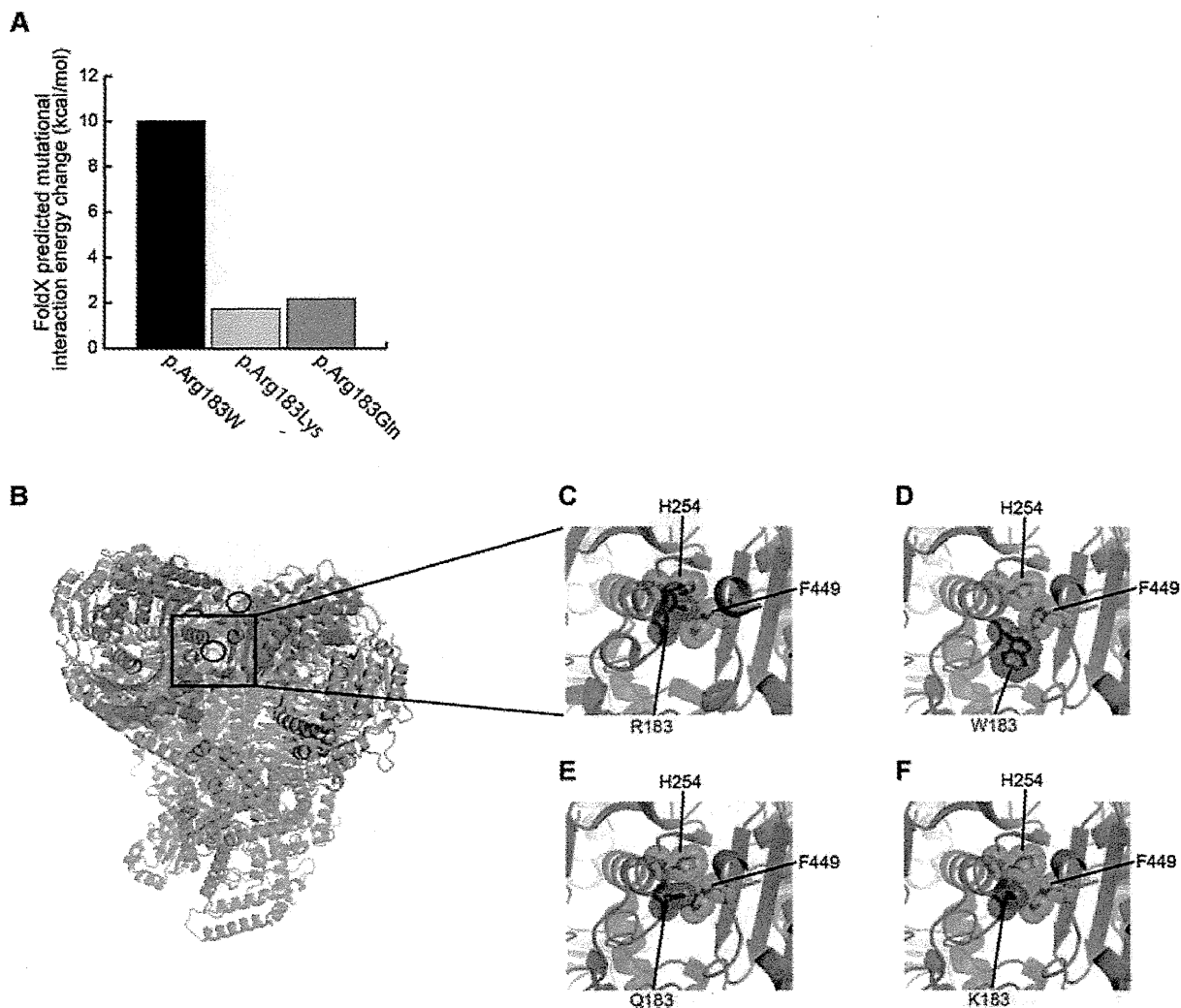


**Figure 2.** Molecular structural consideration of the effect on dimerization of amino acid replacement at residue position 183 in the core protein. **A:** Calculated interaction-energy change of the core protein homodimer upon replacement by the indicated amino acids at residue 183 using FoldX software. **B:** Overview of the crystal structure of the bovine mitochondrial bc1 (CIII) complex (PDB code 2A06). The core protein monomers are colored green and cyan; the other components are shown in gray. The helices, strands, and loops are shown as ribbons, arrows, and threads, respectively. The red circle indicates residue 183 in the core protein. The box corresponds to the enlarged areas shown in parts (C)–(F). **C–F:** Detailed views of the core protein homodimerization interface in the wild-type (C) and mutated, polymorphic, orthologous (p.Arg183Trp/Gln/Lys) (D, E, F, respectively) complex structures. The residues at amino acid 183 of one subunit (red), and His254 and Phe449 of the other subunit (orange) are shown as sticks with Connolly surfaces. All graphics were drawn using PyMOL ([www.pymol.com](http://www.pymol.com)).

using mitochondrial fractions prepared from primary fibroblasts derived from patient 1. With normalization to complex II activity, the CIII activity of patient 1 was decreased to 50% of that in the control subjects ( $n = 10$ ), whereas complex I activity increased by threefold and complex IV activity remained at the same level as in the control subjects (Fig. 3A). Similar results were obtained using normalization to citrate synthase activity (Fig. 3B). We also investigated the steady-state level of the respiratory complexes by blue-native polyacrylamide gel electrophoresis (BN-PAGE) using the same mitochondrial fraction used for the enzyme activity measurements. For analysis of individual complexes, mitochondria were solubilized with 0.5% (w/v) DDM. For analysis of the supercomplex (complexes I, III, and IV), mitochondria were solubilized with 1% (w/v) digitonin. After BN-PAGE, we performed immunoblotting with specific antibodies for the respi-

ratory complexes (Fig. 3C–F, Supp. Notes, and Supp. Fig. S4). In the patient's fibroblasts, we found that CIII and supercomplex assembly were decreased to 18%–20%  $\gg$  22%–23% (Fig. 3C and D) and 4%  $\gg$  7.5% (Fig. 3E and F) of the levels in pooled control samples, respectively. These data indicate that a homozygous missense mutation (c.547C>T, p.Arg183Trp) in *UQCRC2* causes moderately impaired CIII function and severely decreased amounts of CIII and supercomplex, which would be the primary molecular pathogenesis in the patients.

## Discussion

Among the genes known to cause CIII deficiency, impairment of *UQCRC2*, as found in our patients, leads to a similar clinical course to that reported for *UQCRB* defects with recurrent crises of

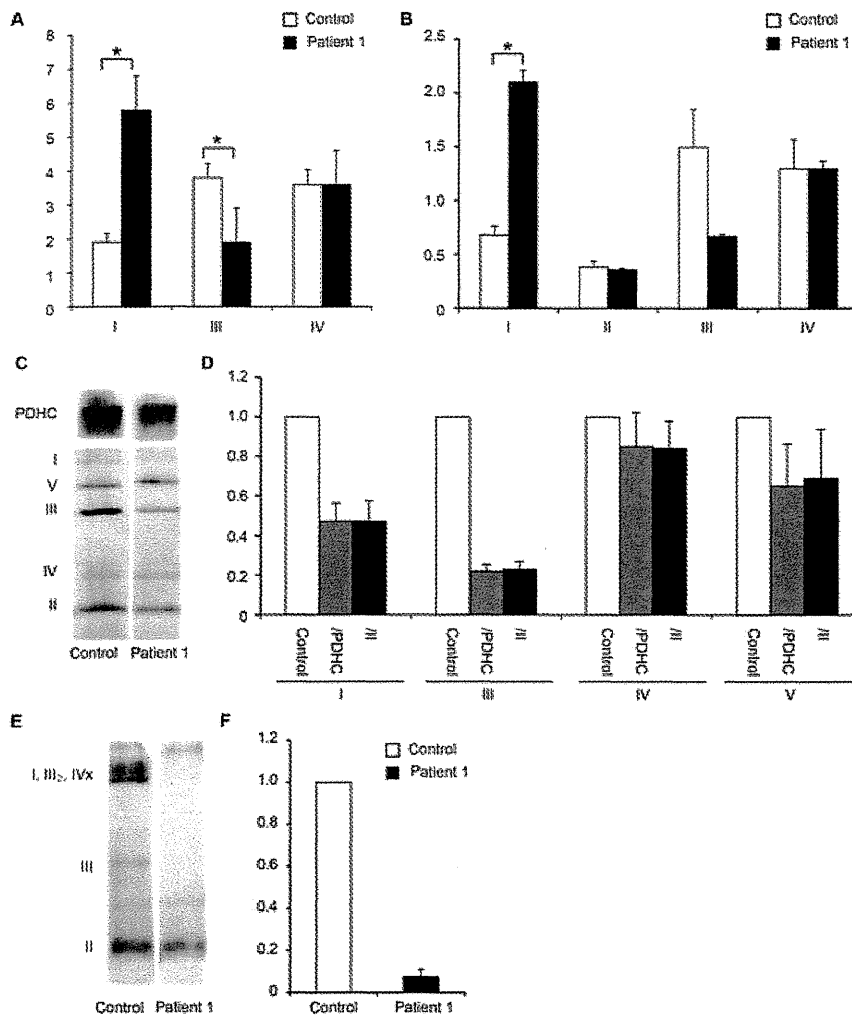


**Figure 3.** Mitochondrial enzyme activity and supercomplex formation. **A, B:** Enzyme activities of the mitochondrial respiratory chain complexes using mitochondrial fractions prepared from primary fibroblasts derived from patient 1 ( $n = 3$ ) and control subjects ( $n = 10$ ). Each measurement was performed in triplicate. The values were normalized to complex II (**A**) or citrate synthase (**B**). Error bars represent the SEM. **C, D:** Immunoblot detection of each respiratory chain complex using mitochondria solubilized with 0.5% DDM. The same amount of pooled mitochondrial protein from control subjects ( $n = 10$ ) was loaded into the control lane. The band intensity of each respiratory complex was estimated by densitometry and normalized to that of PDHC (gray bar) or complex II (black bar). The data were obtained by three independent assays and the error bars in (**D**) represent the SEM. **E, F:** Immunoblot detection of the respiratory supercomplex using mitochondria solubilized with 1% (w/v) digitonin. The same amount of pooled mitochondrial protein from control subjects ( $n = 10$ ) was loaded into the control lane. The band intensity of the supercomplex was estimated by densitometry and normalized to that of complex II (black bar). The data were obtained by three independent assays and the error bars in (**F**) represent the SEM.

hypoglycemia, lactic acidosis, and ketosis, although the latter did not show hyperammonemia. In contrast, impairment of BCS1L, TTC19, and UQCRC2 leads to rather severe complications such as intrauterine growth retardation, liver failure, tubulopathy, sensorineural hearing loss, and abnormalities on brain MRI. The normal development in our patients, despite frequent metabolic crises, may suggest that the UQCRC2 phenotype in our family is milder than disorders of the CIII genes and that this UQCRC2 abnormality does not primarily affect the brain. However, patients 2 and 3 showed epilepsy, and developmental delay was noted in patient 3. It remains to be seen whether this clinical variability is caused by variable expressivity, unknown modifiers, or secondary to the severity of the acute metabolic crises. Interestingly, our patients showed hyperammonemia, highly abnormal urine organic acids indicative

of mitochondrial dysfunction, and highly elevated plasma hydroxyl fatty acids during their crises, whereas patients with the other reported CIII impairment disorders did not [Barel et al., 2008; de Lonlay et al., 2001; Ghezzi et al., 2011; Haut et al., 2003; Hinson et al., 2007; Visapaa et al., 2002]. These observations may imply that UQCRC2 mutations have secondary effects in other metabolic pathways including the Krebs cycle, beta oxidation, and urea cycle.

## Conclusion

We have identified, for the first time, a homozygous mutation in human UQCRC2 encoding a core protein of mitochondrial CIII. Further studies of additional patients with UQCRC2 abnormalities are necessary to fully understand human CIII disorders.

## Acknowledgments

We thank all the family members for participating in this study. We also thank the Commission for Families and Children of Orange County for its support of our clinical work. We appreciate Dr. Takeyori Saheki for useful comments on metabolic decompensation. This study was performed at the Advanced Medical Research Center, Yokohama City University.

*Disclosure statement:* The authors have no conflict of interest to declare.

## References

- Barel O, Shorer Z, Flusser H, Ofir R, Narkis G, Finer G, Shalev H, Nasasra A, Saada A, Birk OS. 2008. Mitochondrial complex III deficiency associated with a homozygous mutation in UQCRCQ. *Am J Hum Genet* 82:1211–1216.
- Benit P, Lebon S, Rustin P. 2009. Respiratory-chain diseases related to complex III deficiency. *Biochim Biophys Acta* 1793:181–185.
- de Lonlay P, Valnot I, Barrientos A, Gorbatyuk M, Tzagoloff A, Taanman JW, Benayoun E, Chretien D, Kadhon N, Lombes A, de Baulny HO, Niaudet P, et al. 2001. A mutant mitochondrial respiratory chain assembly protein causes complex III deficiency in patients with tubulopathy, encephalopathy and liver failure. *Nat Genet* 29:57–60.
- DiMauro S, Schon EA. 2003. Mitochondrial respiratory-chain diseases. *N Engl J Med* 348:2656–2668.
- Fernandez-Vizarra E, Bugiani M, Goffrini P, Carrara F, Farina L, Procopio E, Donati A, Uziel G, Ferrero I, Zeviani M. 2007. Impaired complex III assembly associated with BCS1L gene mutations in isolated mitochondrial encephalopathy. *Hum Mol Genet* 16:1241–1252.
- Ghezzi D, Arzuffi P, Zordan M, Da Re C, Lamperti C, Benna C, D'Adamo P, Diodato D, Costa R, Mariotti C, Uziel G, Smiderle C, et al. 2011. Mutations in TTC19 cause mitochondrial complex III deficiency and neurological impairment in humans and flies. *Nat Genet* 43:259–263.
- Gudbjartsson DF, Thorvaldsson T, Kong A, Gunnarsson G, Ingolfsdottir A. 2005. Allegro version 2. *Nat Genet* 37:1015–1016.
- Guerois R, Nielsen JE, Serrano L. 2002. Predicting changes in the stability of proteins and protein complexes: a study of more than 1000 mutations. *J Mol Biol* 320:369–387.
- Haut S, Brivet M, Touati G, Rustin P, Lebon S, Garcia-Cazorla A, Saudubray JM, Boutron A, Legrand A, Slama A. 2003. A deletion in the human QP-C gene causes a complex III deficiency resulting in hypoglycaemia and lactic acidosis. *Hum Genet* 113:118–122.
- Hinson JT, Fantin VR, Schonberger J, Breivik N, Siem G, McDonough B, Sharma P, Keogh I, Godinho R, Santos F, Esparza A, Nicolau Y, et al. 2007. Missense mutations in the BCS1L gene as a cause of the Bjornstad syndrome. *N Engl J Med* 356:809–819.
- Iwata S, Lee JW, Okada K, Lee JK, Iwata M, Rasmussen B, Link TA, Ramaswamy S, Jay BK. 1998. Complete structure of the 11-subunit bovine mitochondrial cytochrome bc1 complex. *Science* 281:64–71.
- Khan S, Vihinen M. 2010. Performance of protein stability predictors. *Hum Mutat* 31:675–684.
- Mitsuhashi S, Hatakeyama H, Karahashi M, Koumura T, Nonaka I, Hayashi YK, Noguchi S, Sher RB, Nakagawa Y, Manfredi G, Goto Y, Cox GA, Nishino I. 2011. Muscle choline kinase beta defect causes mitochondrial dysfunction and increased mitophagy. *Hum Mol Genet* 20:3841–3851.
- Schagger H, Pfeiffer K. 2000. Supercomplexes in the respiratory chains of yeast and mammalian mitochondria. *EMBO J* 19:1777–1783.
- Trounce IA, Kim YL, Jun AS, Wallace DC. 1996. Assessment of mitochondrial oxidative phosphorylation in patient muscle biopsies, lymphoblasts, and transmittochondrial cell lines. *Methods Enzymol* 264:484–509.
- Tsurusaki Y, Osaka H, Hamanoue H, Shimbo H, Tsuji M, Doi H, Saitsu H, Matsumoto N, Miyake N. 2011. Rapid detection of a mutation causing X-linked leucoencephalopathy by exome sequencing. *J Med Genet* 48:606–609.
- Visapaa I, Fellman V, Vesa J, Dasvarma A, Hutton JL, Kumar V, Payne GS, Makarow M, Van Coster R, Taylor RW, Turnbull DM, Suomalainen A, et al. 2002. GRACILE syndrome, a lethal metabolic disorder with iron overload, is caused by a point mutation in BCS1L. *Am J Hum Genet* 71:863–876.



## *De novo* mutations in the autophagy gene *WDR45* cause static encephalopathy of childhood with neurodegeneration in adulthood

Hirotomo Saito<sup>1,10</sup>, Taki Nishimura<sup>2,3,10</sup>, Kazuhiro Muramatsu<sup>4,10</sup>, Hirofumi Kodera<sup>1</sup>, Satoko Kumada<sup>5</sup>, Kenji Sugai<sup>6</sup>, Emi Kasai-Yoshida<sup>5</sup>, Noriko Sawaura<sup>4</sup>, Hiroya Nishida<sup>7</sup>, Ai Hoshino<sup>7</sup>, Fukiko Ryujin<sup>8</sup>, Seiichiro Yoshioka<sup>8</sup>, Kiyomi Nishiyama<sup>1</sup>, Yukiko Kondo<sup>1</sup>, Yoshinori Tsurusaki<sup>1</sup>, Mitsuko Nakashima<sup>1</sup>, Noriko Miyake<sup>1</sup>, Hirokazu Arakawa<sup>4</sup>, Mitsuhiro Kato<sup>9</sup>, Noboru Mizushima<sup>2,3</sup> & Naomichi Matsumoto<sup>1</sup>

Static encephalopathy of childhood with neurodegeneration in adulthood (SENDA) is a recently established subtype of neurodegeneration with brain iron accumulation (NBIA)<sup>1–3</sup>. By exome sequencing, we found *de novo* heterozygous mutations in *WDR45* at Xp11.23 in two individuals with SENDA, and three additional *WDR45* mutations were identified in three other subjects by Sanger sequencing. Using lymphoblastoid cell lines (LCLs) derived from the subjects, aberrant splicing was confirmed in two, and protein expression was observed to be severely impaired in all five. *WDR45* encodes WD-repeat domain 45 (WDR45). *WDR45* (also known as WIPI4) is one of the four mammalian homologs of yeast Atg18, which has an important role in autophagy<sup>4,5</sup>. Lower autophagic activity and accumulation of aberrant early autophagic structures were demonstrated in the LCLs of the affected subjects. These findings provide direct evidence that an autophagy defect is indeed associated with a neurodegenerative disorder in humans.

NBIA is a heterogeneous group of neurodegenerative diseases that are characterized by a prominent extrapyramidal movement disorder, intellectual deterioration and deposition of iron in the basal ganglia<sup>1–3</sup>. Mutations in several genes involved in diverse cellular processes cause NBIA<sup>6</sup>. SENDA is a recently established subtype of NBIA. SENDA begins with early childhood psychomotor retardation, which remains static until adulthood. Then, during their twenties to early thirties, affected individuals develop sudden-onset progressive dystonia-parkinsonism and dementia. In addition to iron deposition in the globus pallidus and substantia nigra, individuals with SENDA have a distinct pattern on brain magnetic resonance images (MRI)

of T1-weighted signal hyperintensity of the substantia nigra, with a central band of hypointensity<sup>1–3,6,7</sup>. SENDA is always sporadic<sup>6,7</sup>, suggesting the involvement of *de novo* mutations or autosomal recessive traits. To identify *de novo* or recessive mutations, family-based exome sequencing was performed including the affected individual, an unaffected sibling and the unaffected parents.

A total of 180 and 187 rare protein-altering and splice-site variants were identified per affected subject, which were absent in dbSNP135 data and in 88 in-house control exomes (Supplementary Table 1). All genes in each subject were surveyed for *de novo* mutations and compound heterozygous or homozygous mutations that were consistent with an autosomal recessive trait in each family (Supplementary Table 2). Two *de novo* and one autosomal recessive candidate mutations were found in subject 1, and a *de novo* candidate mutation was found in subject 2. Only mutations in *WDR45* at Xp11.23, encoding *WDR45* (referred to here as WIPI4), were common in the two subjects. A canonical splice-site mutation (c.439+1G>T) was found in subject 1, and a synonymous mutation located at the last base of exon 8 (c.516G>C) was found in subject 2, both of which occurred *de novo* (Fig. 1a). Sanger sequencing of *WDR45* in three other affected subjects identified one nonsense and two frameshift mutations (Fig. 1a). The c.1033\_1034dupAA mutation in subject 5 occurred *de novo*. Parental samples for the other two subjects were unavailable. None of the five mutations were found in 6,500 National Heart, Lung, and Blood Institute (NHLBI) exomes or among our 212 in-house control exomes. All subjects with a *WDR45* mutation are female.

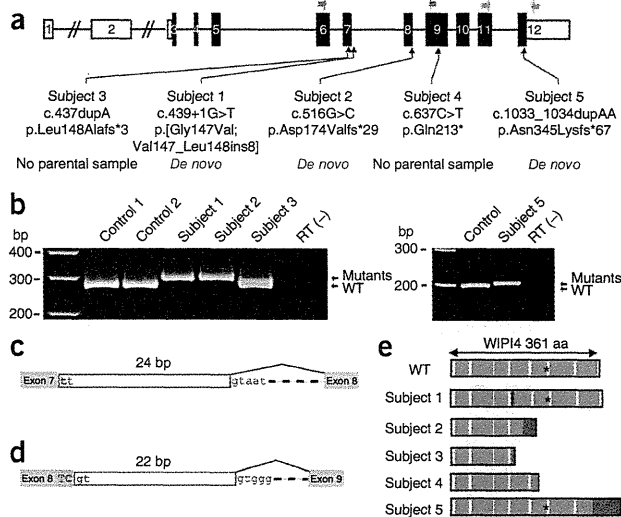
To examine the effects of the mutations on *WDR45* transcription, RT-PCR and sequencing were performed on total RNA extracted from the LCLs of subjects. The c.439+1G>T mutation in subject 1 and the c.516G>C mutation in subject 2 caused 24-bp in-frame and 22-bp

<sup>1</sup>Department of Human Genetics, Graduate School of Medicine, Yokohama City University, Yokohama, Japan. <sup>2</sup>Department of Physiology and Cell Biology, Graduate School and Faculty of Medicine, Tokyo Medical and Dental University, Tokyo, Japan. <sup>3</sup>Department of Biochemistry and Molecular Biology, Graduate School and Faculty of Medicine, The University of Tokyo, Tokyo, Japan. <sup>4</sup>Department of Pediatrics, Gunma University Graduate School of Medicine, Gunma, Japan. <sup>5</sup>Department of Neuropediatrics, Tokyo Metropolitan Neurological Hospital, Tokyo, Japan. <sup>6</sup>Department of Child Neurology, National Center of Neurology and Psychiatry, Tokyo, Japan. <sup>7</sup>Department of Pediatrics, National Rehabilitation Center for Children with Disabilities, Tokyo, Japan. <sup>8</sup>Department of Pediatrics, Shiga University of Medical Science, Shiga, Japan. <sup>9</sup>Department of Pediatrics, Yamagata University Faculty of Medicine, Yamagata, Japan. <sup>10</sup>These authors contributed equally to this work. Correspondence should be addressed to H.S. (hsaito@yokohama-cu.ac.jp), N. Mizushima (nmizu@m.u-tokyo.ac.jp) or N. Matsumoto (naomat@yokohama-cu.ac.jp).

Received 24 October 2012; accepted 29 January 2013; published online 24 February 2013; doi:10.1038/ng.2562



**Figure 1** Heterozygous *WDR45* mutations in individuals with SENDA. (a) Schematic of *WDR45*, which comprises 12 exons (rectangles). The UTRs and coding region are shown in white and black, respectively. Three mutations were confirmed as *de novo*; the others were unable to be confirmed because parental samples were unavailable. Blue and green arrows indicate the locations of the two sets of primers used in mRNA analysis. (b) RT-PCR analysis using the blue primer set (left) and green primer set (right) from a. Whereas control cDNA samples showed a single product corresponding to the wild-type allele (WT), an apparently longer product was observed in subjects 1, 2 and 5, indicating that only the transcripts from the mutant allele were expressed. In subject 3, both wild-type and mutant alleles were expressed. Template without reverse transcriptase was used as a negative control, RT(-). (c) Schematic of the mutant transcript resulting from the c.439+1G>T mutation (red) in subject 1. A 24-bp insertion caused by the use of a cryptic splice donor site within intron 7 was observed, resulting in a p.Gly147Val substitution followed by an in-frame eight-amino-acid insertion (p.[Gly147Val; Val147\_Leu148ins8]). (d) Schematic of the mutant transcript resulting from the c.516G>C mutation (red) in subject 2. A 22-bp insertion from the use of a cryptic splice donor site within intron 8 was observed, leading to a frameshift (p.Asp174Valfs\*29). (e) Schematic of mutant WIPI4 proteins.  $\beta$ -propeller structures and additional residues caused by mutations are colored in blue and red, respectively. The amino-acid residues of the mutant protein predicted from cDNA sequences are shown in relation to seven- $\beta$  propeller structures<sup>13–15</sup>. An asterisk indicates the position of the FRRG motifs.



frameshift insertions, respectively (Fig. 1b–d and Supplementary Fig. 1). The c.437dupA, c.637C>T and c.1033\_1034dupAA mutations were confirmed in the transcripts (Fig. 1b and Supplementary Fig. 1). Theoretically, mutant WIPI4 would be severely truncated in subjects 2, 3 and 4 and relatively conserved in subjects 1 and 5 (Fig. 1e). As human female cells are subject to X-chromosome inactivation, subjects with a *WDR45* mutation may have two cell populations: one expressing a wild-type allele and the other expressing a mutant allele. Notably, whereas both wild-type and mutant alleles were expressed in the LCLs of subject 3, the LCLs of the other four affected subjects exclusively expressed mutant transcripts, suggesting that the wild-type alleles underwent X inactivation in most cells (Fig. 1b and Supplementary Fig. 1). In fact, X-inactivation analysis with genomic DNA from peripheral leukocytes showed a skewed pattern in subjects 2, 4 and 5 (analysis was non-informative in subject 1) (Supplementary Table 3). However, it is unknown whether the wild-type allele underwent X inactivation in brain tissues as in LCLs and leukocytes from the subjects.

The clinical features of the individuals with SENDA possessing *WDR45* mutations are summarized in Table 1 (see also the Supplementary Note). Subjects 1 and 3 have been described recently<sup>7,8</sup>. These individuals showed psychomotor developmental delay from infancy and severe intellectual disability, while their motor function gradually developed. In adulthood, severe progressive dystonia-parkinsonism and dementia developed. Four of the subjects became bedridden within a few years of onset of cognitive decline. In all subjects, blood concentrations of ceruloplasmin, copper, iron, ferritin and lactate acid were normal. Brain MRI showed T1-weighted signal hyperintensity in the substantia nigra with a central T1-weighted hypointensity band (Fig. 2a–e) and T2-weighted signal hypointensity, suggesting iron deposition in the globus pallidus and substantia nigra (Fig. 2f–h), which are characteristic of SENDA. In addition, significant cerebral atrophy was found (Fig. 2i,j). Substantial differences in the severity of clinical findings were not observed among the five subjects.

WIPI1, WIPI2, WIPI3 and WIPI4, mammalian Atg18 homologs, have an important role in the autophagy pathway<sup>4,5</sup>. Autophagy is the major intracellular degradation system by which cytoplasmic materials are enclosed by double-membrane structures called

autophagosomes and subsequently delivered to lysosomes for degradation<sup>9</sup>. More than 30 autophagy-related (ATG) genes have been identified in yeast<sup>10,11</sup>, many of which are conserved in higher eukaryotes and are essential for the formation of the autophagosome<sup>10,12</sup>. These factors include subunits of the class III phosphatidylinositol 3-kinase complex, and generation of the lipid phosphatidylinositol 3-phosphate is essential for autophagosome formation. Atg18 in yeast and WIPI subunits in mammals associate with membranes through a phosphoinositide-binding motif (FRRG) within a seven- $\beta$  propeller structure<sup>13–15</sup>. Atg18 and WIPI proteins also interact with Atg2 and its homologs in yeast and mammalian cells, respectively<sup>16,17</sup>. Autophagic activity in relation to WIPI4 expression was examined using LCLs from the subjects. Immunoblot analysis of WIPI4 showed lower expression in all five subjects compared to unaffected individuals (Fig. 3a). Although mutant WIPI4 protein sequence was relatively conserved in subjects 1 and 5, the expression of mutant WIPI4 in both subjects was severely decreased, similar to that of subjects 2, 3 and 4, in whom mutant WIPI4 was truncated. This suggests that all the mutant proteins are structurally unstable and undergo degradation. To examine the effect of the *WDR45* mutations on autophagy, an autophagic flux assay was performed using LCLs. When lysosomal degradation was blocked by the lysosomal inhibitor chloroquine, the amount of LC3-II (the membrane-bound form) was higher than in cells without the inhibitor, as for control LCLs (Fig. 3b and Supplementary Fig. 2)<sup>18</sup>. The differences in LC3-II amounts between samples with and without chloroquine represent the amount of LC3 on autophagic structures delivered to lysosomes for degradation<sup>18</sup>. In the LCLs from affected subjects, accumulation of LC3-II was observed, even under normal conditions, which was more apparent when autophagy was induced by the mTORC1 inhibitor Torin1 (Supplementary Fig. 2a–d). The increase in the LC3-II amount by concomitant chloroquine treatment was significant or tended to be suppressed in the LCLs from affected subjects, suggesting that the autophagic flux was blocked, probably incompletely, at an intermediate step of autophagosome formation (Fig. 3b and Supplementary Fig. 2e).

Consistent with the immunoblot analysis, immunofluorescence microscopy showed the accumulation of LC3-containing autophagic

**Table 1 Clinical features of subjects with SENDA with a *WDR45* mutation**

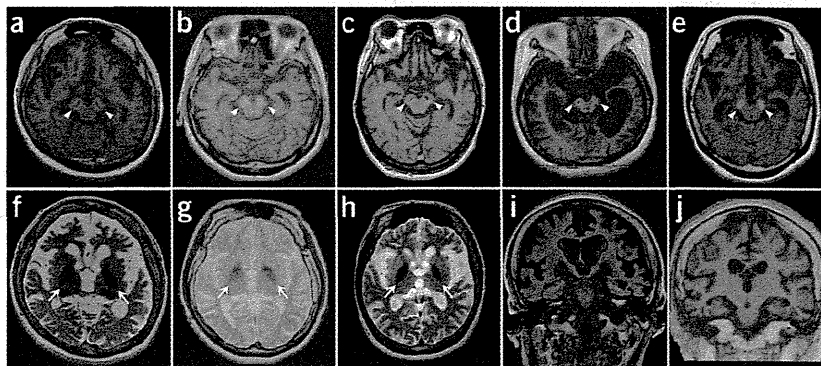
	Subject 1	Subject 2	Subject 3	Subject 4	Subject 5
Age	33 years	28 years	40 years	51 years	33 years
Sex	Female	Female	Female	Female	Female
Mutation	c.439+1G>T	c.516G>C	c.437dupA	c.637C>T	c.1033_1034dupAA
Protein alteration	p.[Gly147Val; Val147_Leu148ins8]	p.Asp174Valfs*29	p.Leu148Alafs*3	p.Gln213*	p.Asn345Lysfs*67
<b>Neurological symptoms</b>					
Current status	Bedridden	Wheelchair	Bedridden	Bedridden	Bedridden
Initial symptom	Psychomotor retardation	Psychomotor retardation	Psychomotor retardation	Psychomotor retardation	Psychomotor retardation
Initial walking	3 years	2 years 7 months	2 years 2 months	1 year 6 months	1 year 6 months
Speech ability	No word	One word	No word	Two-word sentences	Few words
Cognitive dysfunction during childhood	Nonprogressive	Nonprogressive	Nonprogressive	Nonprogressive	Nonprogressive
Start of cognitive decline	26 years	25 years	30 years	24 years	23 years
Period until bedridden after decline	4 years	–	3 years	1 year	6 years
Dystonia	+	+	+	+	+
Parkinsonism	Rigidity, akinesia	Rigidity, akinesia	Rigidity	Rigidity	Rigidity, tremor, impairment of postural reflex
Progressive dementia during adulthood	+	+	+	+	+
Psychiatric symptoms	Aggressive behaviors	Aggressive behaviors	None	None	Anxiety
Epileptic seizure	+	+	FS	None	+
<b>Radiological features</b>					
<b>MRI</b>					
Iron deposition	Globus pallidus, substantia nigra	Globus pallidus, substantia nigra	Globus pallidus, substantia nigra	Globus pallidus, substantia nigra	Globus pallidus, substantia nigra
Central band of T1 hypointensity	+	+	+	+	+
Cerebral atrophy	Moderate at 25 years, remarkable at 32 and 33 years	Moderate at 25 and 27 years	Mild at 33 years, remarkable at 39 years	Mild at 27 years, remarkable at 46 years	Remarkable at 33 years
Eye of the tiger sign	–	–	–	–	–
White matter involvement	–	–	–	–	–
Cerebellar atrophy	Mild at 25, 32 and 33 years	Mild at 25 and 27 years	Mild at 33 and 39 years	Mild at 27 and 46 years	Mild at 33 years
<b>CT findings</b>					
	High density in globus pallidus	Mild high density in substantia nigra	High density in substantia nigra	High density in ventral midbrain	High density in globus pallidus
<b>Neurophysiological examination</b>					
EEG	Bilateral frontal spike	Bilateral frontal spike, low voltage, slow wave	Low voltage	Abnormal	Abnormal
EMG	NE	NE	Dystonic pattern	Normal	NE
VEP	Normal	NE	Prolonged P100 latency	NE	Normal
ABR	Low amplitude, normal latency	NE	No response at 100 dB	NE	NE

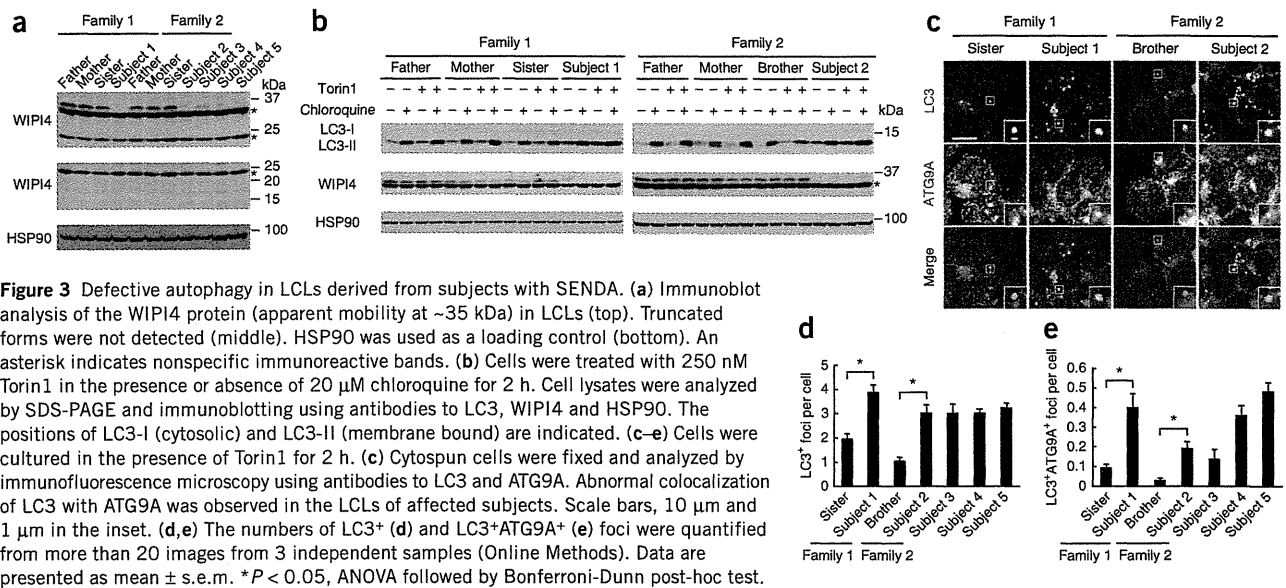
FS, febrile seizure; EEG, electroencephalogram; EMG, electromyogram; VEP, visual evoked potential; ABR, auditory brainstem response; NE, not examined.

structures in the LCLs from affected subjects, some of which were abnormally enlarged compared with those observed in control LCLs (Fig. 3c,d). Therefore, we examined whether these LC3-positive

structures in fact included premature or abnormal autophagic structures. A recent study showed that knockdown of *Wdr45* in rat kidney cells and mutation in *epg-6* (encoding a WIPI4 homolog)

**Figure 2** Brain MRIs at 3.0 T and 1.5 T. (a–e) T1-weighted imaging shows hyperintensity of the substantia nigra with a central band of T1-weighted hypointensity (arrowheads). Images are shown for subject 1 at 33 years (a), subject 2 at 25 years (b), subject 3 at 39 years (c), subject 4 at 46 years (d) and subject 5 at 33 years (e). (f–h) T2-weighted imaging shows marked hypointensity of the globus pallidus (arrows), suggesting iron deposition. Cerebral atrophy and mild cerebellar atrophy are also seen. Images are shown for subject 1 (f), subject 2 (g) and subject 3 (h). (i, j) The fluid attenuated inversion recovery (FLAIR) image of subject 1 (i) and the T1-weighted FLAIR coronal image of subject 2 (j) also show cerebral atrophy.





in *Caenorhabditis elegans* cause accumulation of early autophagic structures<sup>5</sup>. One supposed function of WIPI4 (Epg-6) is to regulate the distribution of ATG9A-marked vesicles<sup>5</sup>, which transiently localize to the autophagosome formation site and induce autophagosome formation<sup>19,20</sup>. ATG9A is absent from completed autophagosomes in mammalian cells; therefore, colocalization of ATG9A and LC3 is rare. However, enlarged structures positive for both ATG9A and LC3 accumulated in LCLs from all five subjects (Fig. 3c,e), indicating improper autophagosome formation.

The importance of the housekeeping activity of autophagy in neurons, as well as the ubiquitin-proteasome system, has been demonstrated in mice. Mice lacking autophagy in the central nervous system developed progressive motor and behavioral deficits<sup>21,22</sup>. Histologically, inclusion bodies containing polyubiquitinated proteins were observed in neurons, and their size and number increased with age<sup>21,22</sup>. Neuronal cell death was observed in subsets of neurons<sup>21,22</sup>, implying that the impairment of autophagy contributes to the pathogenesis of neurodegenerative disorders. Indeed, dysregulation of autophagy has been suggested in various neurodegenerative disorders in humans<sup>23</sup>. In addition, mutations in *PARK2* and *PINK1*, both of which cause familial Parkinson's disease<sup>24,25</sup>, impair the selective autophagic degradation of damaged mitochondria, called mitophagy (*PARK2*, also called Parkin, is recruited to damaged mitochondria in a *PINK1*-dependent manner)<sup>26,27</sup>. However, a direct link between the core autophagy machinery and human neurodegenerative disorders has not been reported. Here, we showed that mutations in *WDR45*, a core autophagy gene, result in a neurodegenerative disorder. Notably, the autophagy defects were partial, implying that some autophagic activity could be maintained in the neurons of affected subjects. We hypothesize that this might be a possible explanation of why childhood intellectual disability in individuals with SENDA remains static until adulthood, unlike in other forms of NBSA<sup>1–3</sup>. In contrast to heterozygous *WDR45* mutations in females, hemizygous germline mutations in males, leading to the expression of mutant *WDR45* in all cells, possibly cause lethal phenotypes from complete loss of *WDR45* function, as mice defective in autophagy die shortly after birth<sup>28–32</sup>. While this paper was under review, Haack *et al.* reported *WDR45* mutations in 20 subjects, including 3 males, 1 of whom possessed

a mutation that was somatic mosaic, supporting the idea that male germline mutations could be lethal<sup>33</sup>.

*WDR45* is widely expressed in human tissues, with the highest expression found in skeletal muscle<sup>34</sup>. Nevertheless, SENDA phenotypes seem to be limited to the brain. These facts may reflect cell type-dependent differences: autophagy could be more important in neurons (non-dividing, terminally differentiated cells) than in LCLs (rapidly dividing cells). In addition, it is possible that the other WIPI homologs (*WIPI1*, *WIPI2* and *WIPI3*) could compensate for the deficiency in *WIPI4* in a cell type-dependent manner, and the relative contribution of *WIPI4* among WIPI factors may be high in neurons.

In conclusion, heterozygous mutations of X-linked *WDR45*, a core autophagy gene, were identified in SENDA, providing direct evidence that an autophagy defect is indeed associated with a neurodegenerative disorder in humans.

**URLs.** NHLBI Exome Sequencing Project, <http://evs.gs.washington.edu/EVS/>; Picard, <http://picard.sourceforge.net/>; SAMtools, <http://samtools.sourceforge.net/>; dbSNP, <http://www.ncbi.nlm.nih.gov/projects/SNP/>.

## METHODS

Methods and any associated references are available in the online version of the paper.

**Accession codes.** Reference sequences are available from GenBank for *Homo sapiens WDR45* transcript variant 1 mRNA (NM\_007075.3) and *WIPI4* isoform 1 (NP\_009006.2).

*Note: Supplementary information is available in the online version of the paper.*

## ACKNOWLEDGMENTS

We would like to thank the individuals with SENDA and their families for their participation in this study. We thank M. Shiina and K. Ogata for their helpful comments on the protein structure. This work was supported by research grants from the Ministry of Health, Labour and Welfare (H.S., N. Miyake and N. Matsumoto), the Japan Science and Technology Agency (N. Matsumoto) and the Strategic Research Program for Brain Sciences (N. Matsumoto) and a Grant-in-Aid for Scientific Research on Innovative Areas (Transcription Cycle) from the Ministry of Education, Culture, Sports, Science and Technology of Japan



(N. Matsumoto), a Grant-in-Aid for Scientific Research from the Japan Society for the Promotion of Science (N. Matsumoto), a Grant-in-Aid for Young Scientists from the Japan Society for the Promotion of Science (H.S. and N. Miyake), the Funding Program for Next-Generation World-Leading Researchers (N. Mizushima) and a grant from the Takeda Science Foundation (N. Miyake, N. Mizushima and N. Matsumoto).

#### AUTHOR CONTRIBUTIONS

H.S., N. Mizushima and N. Matsumoto designed and directed the study. H.S., T.N., K.M., N. Mizushima and N. Matsumoto wrote the manuscript. K.M., S.K., K.S., E.K.-Y., N.S., H.N., A.H., F.R., S.Y., H.A. and M.K. collected samples and provided the subjects' clinical information. H.S., H.K., K.N., Y.T., M.N. and N. Miyake performed exome sequencing and Sanger sequencing. H.S. and K.N. performed the RNA analysis. Y.K. performed the X-inactivation analysis. T.N. and N. Mizushima analyzed protein expression and autophagic activity.

#### COMPETING FINANCIAL INTERESTS

The authors declare no competing financial interests.

Reprints and permissions information is available online at <http://www.nature.com/reprints/index.html>.

- Gregory, A., Polster, B.J. & Hayflick, S.J. Clinical and genetic delineation of neurodegeneration with brain iron accumulation. *J. Med. Genet.* **46**, 73–80 (2009).
- Kruer, M.C. *et al.* Neuroimaging features of neurodegeneration with brain iron accumulation. *AJNR Am. J. Neuroradiol.* **33**, 407–414 (2012).
- Schneider, S.A. & Bhatia, K.P. Syndromes of neurodegeneration with brain iron accumulation. *Semin. Pediatr. Neurol.* **19**, 57–66 (2012).
- Polson, H.E. *et al.* Mammalian Atg18 (WIPI2) localizes to omegasome-anchored phagophores and positively regulates LC3 lipidation. *Autophagy* **6**, 506–522 (2010).
- Lu, Q. *et al.* The WD40 repeat PtdIns(3)P-binding protein EPG-6 regulates progression of omegasomes to autophagosomes. *Dev. Cell* **21**, 343–357 (2011).
- Gregory, A. & Hayflick, S.J. Genetics of neurodegeneration with brain iron accumulation. *Curr. Neurol. Neurosci. Rep.* **11**, 254–261 (2011).
- Kimura, Y. *et al.* MRI, MR spectroscopy, and diffusion tensor imaging findings in patient with static encephalopathy of childhood with neurodegeneration in adulthood (SENDA). *Brain Dev.* published online; doi:10.1016/j.braindev.2012.07.008 (11 August 2012).
- Kasai-Yoshida, E. *et al.* First video report of static encephalopathy of childhood with neurodegeneration in adulthood. *Mov. Disord.* published online; doi:10.1002/mds.25158 (6 February 2013).
- Mizushima, N. & Komatsu, M. Autophagy: renovation of cells and tissues. *Cell* **147**, 728–741 (2011).
- Nakatogawa, H., Suzuki, K., Kamada, Y. & Ohsumi, Y. Dynamics and diversity in autophagy mechanisms: lessons from yeast. *Nat. Rev. Mol. Cell Biol.* **10**, 458–467 (2009).
- Xie, Z. & Klionsky, D.J. Autophagosome formation: core machinery and adaptations. *Nat. Cell Biol.* **9**, 1102–1109 (2007).
- Mizushima, N., Yoshimori, T. & Ohsumi, Y. The role of Atg proteins in autophagosome formation. *Annu. Rev. Cell Dev. Biol.* **27**, 107–132 (2011).
- Baskaran, S., Ragusa, M.J., Boura, E. & Hurley, J.H. Two-site recognition of phosphatidylinositol 3-phosphate by PROPPINs in autophagy. *Mol. Cell* **47**, 339–348 (2012).
- Krick, R. *et al.* Structural and functional characterization of the two phosphoinositide binding sites of PROPPINs, a  $\beta$ -propeller protein family. *Proc. Natl. Acad. Sci. USA* **109**, E2042–E2049 (2012).
- Watanabe, Y. *et al.* Structure-based analyses reveal distinct binding sites for Atg2 and phosphoinositides in Atg18. *J. Biol. Chem.* **287**, 31681–31690 (2012).
- Suzuki, K., Kubota, Y., Sekito, T. & Ohsumi, Y. Hierarchy of Atg proteins in pre-autophagosomal structure organization. *Genes Cells* **12**, 209–218 (2007).
- Velikkakath, A.K., Nishimura, T., Oita, E., Ishihara, N. & Mizushima, N. Mammalian Atg2 proteins are essential for autophagosome formation and important for regulation of size and distribution of lipid droplets. *Mol. Biol. Cell* **23**, 896–909 (2012).
- Mizushima, N., Yoshimori, T. & Levine, B. Methods in mammalian autophagy research. *Cell* **140**, 313–326 (2010).
- Itakura, E., Kishi-Itakura, C., Koyama-Honda, I. & Mizushima, N. Structures containing Atg9A and the ULK1 complex independently target depolarized mitochondria at initial stages of Parkin-mediated mitophagy. *J. Cell Sci.* **125**, 1488–1499 (2012).
- Orsi, A. *et al.* Dynamic and transient interactions of Atg9 with autophagosomes, but not membrane integration, are required for autophagy. *Mol. Biol. Cell* **23**, 1860–1873 (2012).
- Hara, T. *et al.* Suppression of basal autophagy in neural cells causes neurodegenerative disease in mice. *Nature* **441**, 885–889 (2006).
- Komatsu, M. *et al.* Loss of autophagy in the central nervous system causes neurodegeneration in mice. *Nature* **441**, 880–884 (2006).
- Menzies, F.M., Moreau, K. & Rubinsztein, D.C. Protein misfolding disorders and macroautophagy. *Curr. Opin. Cell Biol.* **23**, 190–197 (2011).
- Valente, E.M. *et al.* Hereditary early-onset Parkinson's disease caused by mutations in *PINK1*. *Science* **304**, 1158–1160 (2004).
- Kitada, T. *et al.* Mutations in the *parkin* gene cause autosomal recessive juvenile parkinsonism. *Nature* **392**, 605–608 (1998).
- Youle, R.J. & van der Bliek, A.M. Mitochondrial fission, fusion, and stress. *Science* **337**, 1062–1065 (2012).
- Youle, R.J. & Narendra, D.P. Mechanisms of mitophagy. *Nat. Rev. Mol. Cell Biol.* **12**, 9–14 (2011).
- Kuma, A. *et al.* The role of autophagy during the early neonatal starvation period. *Nature* **432**, 1032–1036 (2004).
- Saitoh, T. *et al.* Loss of the autophagy protein Atg16L1 enhances endotoxin-induced IL-1 $\beta$  production. *Nature* **456**, 264–268 (2008).
- Saitoh, T. *et al.* Atg9a controls dsDNA-driven dynamic translocation of STING and the innate immune response. *Proc. Natl. Acad. Sci. USA* **106**, 20842–20846 (2009).
- Sou, Y.S. *et al.* The Atg8 conjugation system is indispensable for proper development of autophagic isolation membranes in mice. *Mol. Biol. Cell* **19**, 4762–4775 (2008).
- Komatsu, M. *et al.* Impairment of starvation-induced and constitutive autophagy in *Atg7*-deficient mice. *J. Cell Biol.* **169**, 425–434 (2005).
- Haack, T.B. *et al.* Exome sequencing reveals *de novo* *WDR45* mutations causing a phenotypically distinct, X-linked dominant form of NBIA. *Am. J. Hum. Genet.* **91**, 1144–1149 (2012).
- Proikas-Cezanne, T. *et al.* WIPI-1 $\alpha$  (WIPI49), a member of the novel 7-bladed WIPI protein family, is aberrantly expressed in human cancer and is linked to starvation-induced autophagy. *Oncogene* **23**, 9314–9325 (2004).

## ONLINE METHODS

**Subjects.** We analyzed five Japanese individuals with SENDA. Diagnosis was made on the basis of clinical features, including psychomotor retardation at early childhood that was static for decades and severe progressive dystonia-parkinsonism and dementia after several decades, as well as characteristic findings on brain MRI scans. Genomic DNA was isolated from blood leukocytes according to standard protocols. The Institutional Review Board of Yokohama City University approved the experimental protocols. Informed consent was obtained for all individuals included in this study in agreement with the requirements of Japanese regulations. Clinical information on the subjects with a *WDR45* mutation is presented in **Table 1** and in the **Supplementary Note**.

**Mutation screening.** Mutation screening of exons 3–12 covering the *WDR45* coding region (of transcript variant 1, GenBank accession NM\_007075.3) was performed by direct sequencing. PCR was performed in a 20- $\mu$ l mixture containing 1  $\mu$ l of genomic DNA, 1 $\times$  PCR Buffer for KOD FX NEO, 0.4 mM of each dNTP, 0.3  $\mu$ M of each primer and 0.4 U of KOD FX NEO polymerase (Toyobo). Details on PCR conditions and primer sequences are given in **Supplementary Table 4**.

**Exome sequencing.** Genomic DNA was captured using the SureSelect Human All Exon v4 kit (51 Mb; Agilent Technologies) and sequenced with four samples per lane on an Illumina HiSeq2000 with 101-bp paired-end reads. Image analysis and base calling were performed by sequence control software real-time analysis and CASAVA software v1.8 (Illumina). Reads were aligned to GRCh37 with Novoalign (Novocraft Technologies). Duplicate reads were marked using Picard (see URLs) and excluded from downstream analysis. After merging the BAM files of all members in each family using SAMtools, local realignments around indels and base quality score recalibration were performed with the Genome Analysis Toolkit (GATK)<sup>35</sup>. Single-nucleotide variants and small indels were identified using the GATK UnifiedGenotyper and filtered according to the Broad Institute's best-practice guidelines (version 3). Variants registered in dbSNP135, which were not flagged as clinically associated, were excluded. Variants that passed the filters were annotated using ANNOVAR<sup>36</sup>.

**RNA analysis.** LCLs were established from five affected subjects and their family members. RT-PCR using total RNA extracted from LCLs was performed as previously described<sup>37</sup>. Briefly, 4  $\mu$ g of total RNA extracted with an RNeasy Plus Mini kit (Qiagen) was subjected to reverse transcription, and 2  $\mu$ l of cDNA was used for PCR. Details on primer sequences and PCR conditions are given in **Supplementary Table 4**. PCR products were electrophoresed in a 10% polyacrylamide gel and sequenced.

**X-inactivation analysis.** The X-inactivation pattern was studied using the human androgen receptor (HUMARA) assay and a fragile X mental retardation (*FRAXA*) locus methylation assay as previously described<sup>38–40</sup>. Briefly, genomic DNA from the subjects, a control male and a control female was digested with two methylation-sensitive enzymes, HpaII and HhaI. Details on PCR conditions and primer sequences are given in **Supplementary Table 4**. Fluorescently labeled products were analyzed on an ABI PRISM 3500 Genetic Analyzer with GeneMapper Software version 4.0 (Applied Biosystems). X-inactivation ratios of less than or equal to 80:20 were considered to represent a random pattern, ratios greater than 80:20 were considered to represent a

skewed pattern, and ratios greater than 90:10 were considered to represent a markedly skewed pattern<sup>38</sup>.

**Cell culture.** LCLs were cultured in RPMI 1640 supplemented with 10% FBS, L-glutamine, tylosin and antibiotic-antimycotic solution in a 5% CO<sub>2</sub> incubator.

**Immunoblotting.** An affinity-purified rabbit polyclonal antibody against WPI4 peptide antigen (CFPDNPRKLFEDTRDNP, amino acids 129–145) was generated by Medical & Biological Laboratories. The specificity of the antibody was tested using lysate from HeLa cells in which *WDR45* was knocked down. For immunoblot analysis, cells were lysed with lysis buffer (50 mM Tris-HCl, pH 7.5, 150 mM NaCl, 1 mM EDTA, 1% Triton X-100, 1 mM phenylmethanesulfonyl fluoride and a protease inhibitor cocktail (Complete EDTA-free protease inhibitor, Roche)). Cell lysates were clarified by centrifugation at 12,000g for 20 min and analyzed by SDS-PAGE and immunoblotting using antibodies to WPI4, LC3 (ref. 41) and HSP90 (BD Transduction Laboratories, 610418). Signal intensities were analyzed using a LAS-3000 mini imaging analyzer and Multi Gauge software version 3.0 (Fujifilm). Contrast and brightness adjustments were applied to the images using Photoshop 7.0.1 (Adobe Systems).

**Fluorescence microscopy.** LCLs were spun onto a glass slide at 500 RPM (28g) for 1 min in a Shandon Cytospin 4 cytofuge (Thermo Electron). Cells were fixed with 4% paraformaldehyde, permeabilized using 50  $\mu$ g/ml digitonin and then stained with antibodies to LC3 (clone 1703, Cosmo Bio) and Atg9A<sup>19</sup>. Cells were observed with a confocal laser microscope (FV1000D IX81, Olympus) using a 60 $\times$  PlanApoN oil immersion lens (1.42 numerical aperture (N.A.), Olympus). For final output, images were processed using Adobe Photoshop 7.0.1 software. The number of staining foci was determined as follows: foci were extracted using the top hat operation (parameter of 300  $\times$  300 pixel area), and a binary image was created. Small foci (with an area of less than 10  $\times$  10 pixels) were removed using an open operation. The number of foci was counted using the integrated morphometry analysis program. False foci were removed by comparison with the original image.

**Statistical analysis.** Differences were analyzed statistically using unpaired *t* tests or analysis of variance (ANOVA) with a Bonferroni-Dunn post-hoc test.

35. DePristo, M.A. *et al.* A framework for variation discovery and genotyping using next-generation DNA sequencing data. *Nat. Genet.* **43**, 491–498 (2011).
36. Wang, K., Li, M. & Hakonarson, H. ANNOVAR: functional annotation of genetic variants from high-throughput sequencing data. *Nucleic Acids Res.* **38**, e164 (2010).
37. Saitsu, H. *et al.* *STXBP1* mutations in early infantile epileptic encephalopathy with suppression-burst pattern. *Epilepsia* **51**, 2397–2405 (2010).
38. Kondo, Y. *et al.* A family of oculofaciocardiodental syndrome (OFCD) with a novel *BCOR* mutation and genomic rearrangements involving *NHS*. *J. Hum. Genet.* **57**, 197–201 (2012).
39. Allen, R.C., Zoghbi, H.Y., Moseley, A.B., Rosenblatt, H.M. & Belmont, J.W. Methylation of HpaII and HhaI sites near the polymorphic CAG repeat in the human androgen-receptor gene correlates with X chromosome inactivation. *Am. J. Hum. Genet.* **51**, 1229–1239 (1992).
40. Carrel, L. & Willard, H.F. An assay for X inactivation based on differential methylation at the fragile X locus, *FMR1*. *Am. J. Med. Genet.* **64**, 27–30 (1996).
41. Hosokawa, N., Hara, Y. & Mizushima, N. Generation of cell lines with tetracycline-regulated autophagy and a role for autophagy in controlling cell size. *FEBS Lett.* **580**, 2623–2629 (2006).



## Pathogenic mutations in two families with congenital cataract identified with whole-exome sequencing

Yukiko Kondo,<sup>1</sup> Hirotomoto Saito,<sup>1</sup> Toshinobu Miyamoto,<sup>2</sup> Byung Joo Lee,<sup>3</sup> Kiyomi Nishiyama,<sup>1</sup> Mitsuko Nakashima,<sup>1</sup> Yoshinori Tsurusaki,<sup>1</sup> Hiroshi Doi,<sup>1</sup> Noriko Miyake,<sup>1</sup> Jeong Hun Kim,<sup>3</sup> Young Suk Yu,<sup>3</sup> Naomichi Matsumoto<sup>1</sup>

<sup>1</sup>Department of Human Genetics, Yokohama City University Graduate School of Medicine, Yokohama 236-0004, Japan;

<sup>2</sup>Department of Obstetrics and Gynecology, Asahikawa Medical College, Asahikawa, Japan; <sup>3</sup>Department of Ophthalmology, Seoul National University College of Medicine, Seoul, Korea

**Purpose:** Congenital cataract is one of the most frequent causes of visual impairment and childhood blindness. Approximately one quarter to one third of congenital cataract cases may have a genetic cause. However, phenotypic variability and genetic heterogeneity hamper correct genetic diagnosis. In this study, we used whole-exome sequencing (WES) to identify pathogenic mutations in two Korean families with congenital cataract.

**Methods:** Two affected members from each family were pooled and processed for WES. The detected variants were confirmed with direct sequencing.

**Results:** WES readily identified a *CRYAA* mutation in family A and a *CRYGC* mutation in family B. The c.61C>T (p.R21W) mutation in *CRYAA* has been previously reported in a family with congenital cataract and microcornea. The novel mutation, c.124delT, in *CRYGC* may lead to a premature stop codon (p.C42Afs\*60).

**Conclusions:** This study clearly shows the efficacy of WES for rapid genetic diagnosis of congenital cataract with an unknown cause. WES will be the first choice for clinical services in the near future, providing useful information for genetic counseling and family planning.

Congenital cataract is one of the most frequent causes of visual impairment and childhood blindness worldwide, with an estimated incidence of 2.49 per 10,000 live births by the age of 1 year in the United Kingdom [1]. Congenital cataract is also the leading cause of treatable blindness in childhood. Good outcomes have been reported in children undergoing surgery before 6 weeks of age in bilateral cases [2]. Early diagnosis in the postnatal unit is important for obtaining good visual function.

Many causes have been considered for congenital cataract: intrauterine infection, exposure to drug or radiation in pregnancy, gene defects, chromosomal disorders, metabolic disease, and trauma [3]. Approximately one quarter to one third of congenital cataract cases may have a genetic cause and often follow a Mendelian inheritance pattern, with autosomal dominant traits more common than autosomal recessive and X-linked traits [4,5]. Inter- and intrafamilial phenotypic variability has been reported in cases of inherited congenital cataract [6,7]. It may occur as an isolated eye anomaly, in association with other ocular anomalies, or as part of a

systemic disorder. Congenital cataracts are caused by mutations in various types of genes: lens-related crystallin genes (*CRYAA*, *CRYAB*, *CRYBB1*, *CRYBB2*, *CRYBB3*, *CRYBA1*, *CRYBA4*, *CRYGC*, *CRYGD*, and *CRYGS*), membrane protein genes (*GJA3*, *GJA8*, *MIP*, and *LIM2*), cytoskeleton-related genes (*BFSPI* and *BFSPI2*), and transcription factor genes (*FOXE3*, *HSF4*, *MAF*, *PITX3*, and *PAX6*) [8]. Weisschuh et al. reported that mutations in crystallin genes occupied 50% of all mutations in known disease-causing genes [9], suggesting that mutations in the crystallin genes are particularly abundant.

Whole-exome sequencing (WES) targeting all the protein-coding genes is powerful and cost-effective for dissecting the genetic basis of diseases [10]. WES is particularly useful for identifying pathogenic mutations for Mendelian disorders for which conventional approaches are difficult (such as when most cases are sporadic).

In this report, we performed WES on two Korean families with congenital cataract inherited in an autosomal dominant fashion. We identified pathogenic mutations in both families and demonstrated the diagnostic utility of WES in congenital cataract.

---

Correspondence to: Naomichi Matsumoto, Department of Human Genetics, Yokohama City University Graduate School of Medicine, Fukuura 3-9, Kanazawa-ku, Yokohama 236-0004, Japan; Phone: +81-45-787-2606; FAX: +81-45-786-5219, email: [naomat@yokohama-cu.ac.jp](mailto:naomat@yokohama-cu.ac.jp)

## METHODS

**Clinical report:** The two Korean families with congenital cataract have been described previously (Figure 1A) [11]. Samples from family A with 6 affected (3 females and 3 males) and 3 unaffected members (1 female and 2 males) and family B with 3 affected (1 female and 2 male) and 1 unaffected (female) members were collected at Seoul National University College of Medicine. In family A, the proband (MC41) was diagnosed with congenital cataract and microphthalmia. Other ocular anomalies were noted, including nystagmus, amblyopia, glaucoma, and esotropia. The cousin of the proband (MC42) showed congenital cataract but no microphthalmia. Nystagmus and amblyopia were also noted. In family B, the older sister (MC13, the proband) and the younger brother (MC14) showed congenital cataract. Other ocular anomalies were found, including nystagmus and amblyopia. Systemic abnormalities, intellectual disability, and developmental malformation were unrecognized, and other possible causes such as trauma, intrauterine infection, exposure to drug or radiation, and metabolic disease were unlikely to be involved in both families.

**Whole-exome sequencing:** Blood was collected from antecubital veins of family members and subsequently treated with a Qiagen Blood and Cell Culture DNA Midi Kit (Qiagen) for preparing genomic DNA of leukocytes. Experimental protocols were approved by the Institutional Review Board for Ethical Issues at Yokohama City University School of Medicine and the Committee for Ethical Issues on the Human Genome and Gene Analysis, Seoul National University. Informed consent was obtained from all individuals.

Because the DNA samples were limited, 1.5 µg of DNA from each of two affected members in the respective families were combined, and were processed using a SureSelect Human All Exon 50 Mb Kit (Agilent Technologies, Santa Clara, CA) to generate exome libraries. The libraries were sequenced with one lane per sample of the flow-cell on an Illumina GAIIX (Illumina Inc., San Diego, CA) with 107-bp paired-end reads, according to the manufacturer's instructions. Image analysis and base calling were performed with Sequence Control Software with Real-Time Analysis (Illumina) and CASAVA software v1.7 (Illumina). Reads were aligned and mapped to the human reference genome sequence (University of California Santa Cruz [UCSC] Genome Browser hg19, National Center for Biotechnology Information [NCBI] genome sequence website build 37) using MAQ [12] and NextGENe software v2.00 with sequence condensation by consolidation (SoftGenetics, State College, PA). Single nucleotide variants (SNVs) were called using MAQ and NextGENe. Small insertions and deletions

were detected using NextGENe. Called SNVs were annotated with SeattleSeq Annotation. Candidate variants were confirmed with Sanger sequencing with a 3130xL or 3500xL Genetic Analyzer (Applied Biosystems, Foster City, CA). The Human Gene Mutation Database (HGMD; Biobases, Wolfenbuettel, Germany) was used to check whether the variants had been previously reported. Polymorphism Phenotyping (PolyPhen-2), Sorting Intolerant from Tolerant (SIFT), and MutationTaster were used to evaluate variants in terms of sequence conservation, chemical change, and likelihood of pathogenicity.

## RESULTS

With WES, we attained more than 86% target coverage by ten reads or more (Appendix 1). We adopted a prioritization schema to identify the pathogenic mutation in each pooled sample as follows (Table 1). First, we excluded the variants registered in the Single Nucleotide Polymorphism database (dbSNP132) or the 1000 Genomes project. Then, SNVs commonly detected with MAQ and NextGENe were selected as highly confident variants. In family A, we identified 671 non-synonymous or canonical splice site change SNVs along with 100 small insertions or deletions. We surveyed these for mutations in the 26 known congenital cataract genes and 19 anophthalmia or microphthalmia genes (Appendix 2). We found a heterozygous mutation (c.61C>T [p.R21W]) in exon 1 of *CRYAA* (NM\_000394.2), which was confirmed with Sanger sequencing (Figure 1B,C; Table 1). The mutation occurred at an evolutionarily conserved amino acid (Figure 1D), and was previously reported in a family with congenital cataract and microcornea [7]. The mutation completely cosegregated with the cataract phenotype in this family (Figure 1A).

In family B, we similarly identified 454 non-synonymous or canonical splice site SNVs, and 135 small insertions or deletions (Table 1). We found a novel heterozygous frameshift mutation, c.124delT (p.C42Afs\*60) in *CRYGC* (NM\_020989.3), and confirmed the presence of the mutation in MC13 but not in MC13b with Sanger sequencing (Figure 1E,F; Table 1). Although we pooled DNA from MC13b and MC13 based on our initial clinical information (Figure 1A), MC13b was actually unaffected (because of an error in information transfer). After the phenotypic information for this family was corrected, the mutation completely cosegregated with the cataract phenotype, as confirmed with Sanger sequencing (Figure 1A). This 1-bp deletion would be expected to result in the insertion of 60 new amino acids after the mutation site with a premature stop codon at position 102 (p.C42Afs\*60). This mutation was not found in the



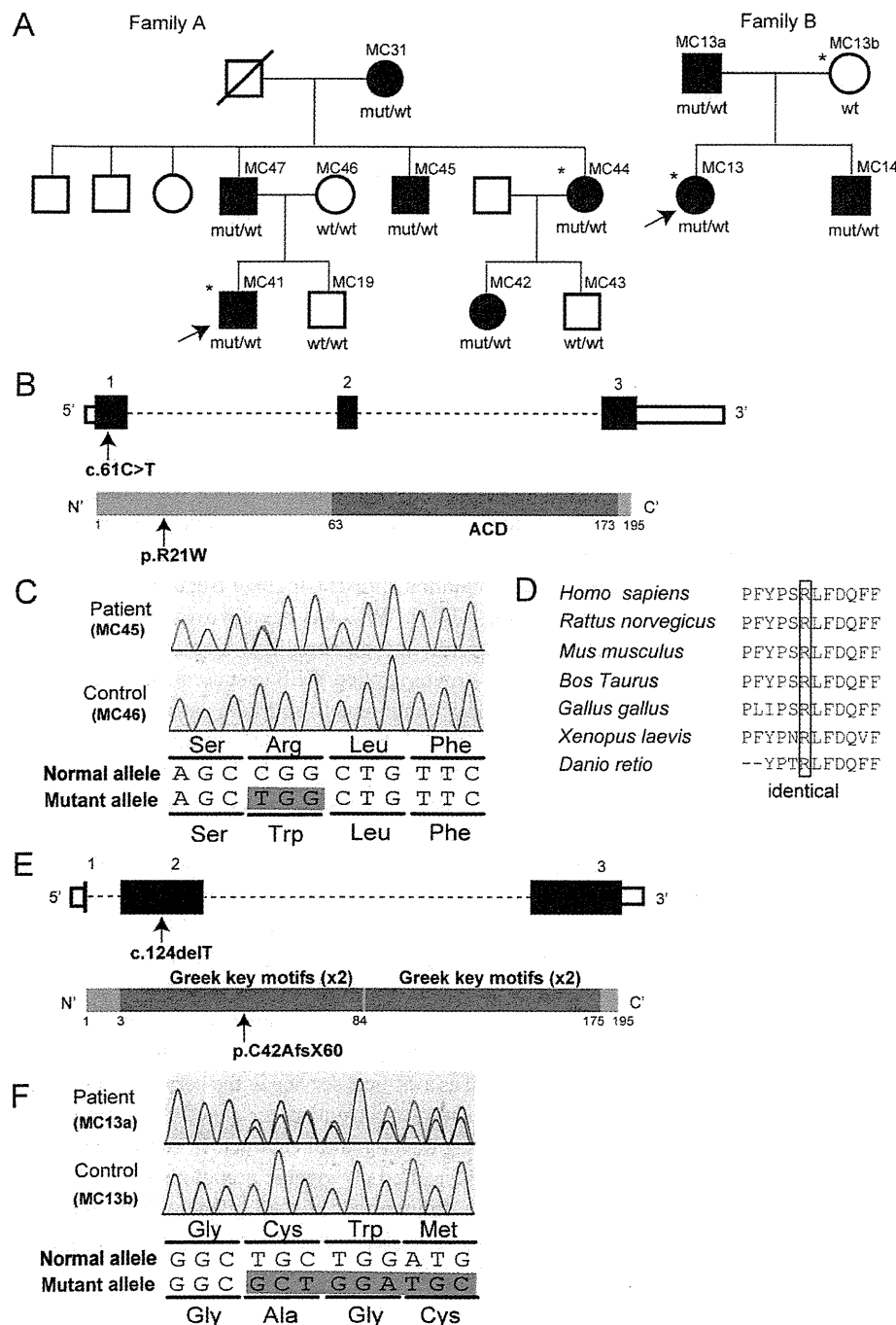


Figure 1. *CRYAA* and *CRYGC* mutations in two Korean families. **A:** Pedigrees of families A and B are indicated. Black and open symbols denote affected and unaffected individuals, respectively. The asterisk shows samples used for whole-exome sequencing. The mutations cosegregate with the phenotype. **B:** Schema of the *CRYAA* gene (top) and the *CRYAA* protein (bottom) is presented. The untranslated regions and coding region are shown as open and filled rectangles, respectively. The location of the c.61C>T mutation is indicated with an arrow. *CRYAA* contains an N-terminal region, an  $\alpha$ -crystallin domain (ACD, dark gray box), and a C-terminal region. **C:** Electropherograms of the mutation in the affected patient (top) and the unaffected control (bottom) are shown. A single nucleotide change in exon 1 results in an amino acid alteration. **D:** The missense mutation occurred at an evolutionarily conserved amino acid. Homologous sequences were aligned using CLUSTALW. **E:** Schema of the *CRYGC* gene (top) and the *CRYGC* protein (bottom) is presented. The untranslated regions and the coding region are shown as open and filled rectangles, respectively. The location of the c.124delT mutation is indicated with an arrow. *CRYGC* contains two domains each composed of two Greek-key motifs (dark gray boxes). **F:** Electropherograms of the *CRYGC* mutation in the affected patient (top) and in the unaffected control (bottom) are shown. A single nucleotide deletion in exon 2 would cause a frameshift. mut, mutant allele; wt, wild-type allele.

National Heart, Lung, and Blood Institute (NHLBI) Exome Sequencing Project (ESP) Exome Variant Server that contains

data from more than 5,400 exomes, or among our in-house exome data from 135 individuals.

TABLE 1. SEQUENCE VARIANTS IN THE TWO FAMILIES FOUND BY WHOLE-EXOME SEQUENCING

	Family A		Family B	
	NextGENe	MAQ	NextGENe	MAQ
Total variant calls	118,801	170,093	130,791	175,155
Unknown SNP variants (dbSNP132, 1000 Genomes project)	28,620	22,038	34,627	21,687
SNVs commonly found by two methods		3,269		2,347
NS+SP (indels) <sup>a</sup>	671	(100)	454	(135)
Present among 45 candidate genes		1		1
Confirmed segregation (heterozygous)		1		1

<sup>a</sup>Small indels were detected only by NextGENe. SNP, single nucleotide polymorphism; SNV, single nucleotide variant; NS, non-synonymous variants; SP, canonical splice site variants; indels, small insertions or deletions.

## DISCUSSION

In this study, a pathogenic mutation in *CRYAA* or *CRYGC*, which encode a crystallin family protein, was identified in each of two Korean families with congenital cataract. Crystallin constitutes the major protein of the vertebrate eye lens and is classified into three main types:  $\alpha$ -,  $\beta$ -, and  $\gamma$ -crystallin. *CRYAA*, encoding  $\alpha$ A-crystallin, maps to chromosome 21q22.3, and mutations have been reported in autosomal dominant congenital cataract [13]. The  $\alpha$ A-crystallin protein consists of an N-terminal region, a conserved  $\alpha$ -crystallin domain, and a short C-terminal region. The  $\alpha$ -crystallin domain may be involved in aggregating and disaggregating larger protein complexes, whereas the N-terminal and the C-terminal regions are suggested to play a role in oligomerization [7,14,15]. The missense mutation found in family A occurred at an evolutionarily conserved amino acid in the N-terminal region, suggesting that the mutation may impair oligomerization. *CRYGC*, encoding  $\gamma$ C-crystallin, plays a crucial role in lens development and the maintenance of lens transparency [16]. The  $\gamma$ C-crystallin proteins are tightly folded into two domains, with each domain composed of two exceptionally stable protein structures called Greek-key motifs [17-19]. The relatively loose or partially unfolded structure of mutant  $\gamma$ C-crystallin may be susceptible to aggregation and insolubilization, which leads to cataract formation [20]. Ren et al. reported a 5-bp duplication (c.119\_123dupGCGGC) within exon 2 of the *CRYGC* gene in patients with autosomal dominant congenital cataract [16]. The c.124delT mutation in family B and the c.119\_123dupGCGGC mutation cause truncation within the first domain, and are likely to lead to similar effects.

We pooled DNA from one unaffected case (MC13b) and one affected case (MC13) in family B because of the error in information transfer (the affected person was switched from MC13a to MC13b), theoretically resulting in one mutant

allele among four existing alleles. However, we still detected a pathological variant (c.124delT), which was present at an allele frequency of 36.47% in our sequence reads. This is consistent with recent reports that WES can detect mosaic pathogenic mutations present at allele frequencies as low as 3.6% to 8% [21-24]. WES has been proven to be useful in clinical diagnosis and personalized disease-risk profiling [10]. Several groups applied WES to successfully identify de novo pathogenic mutations in sporadic patients, supporting its utility [25-27]. WES is particularly useful for small pedigrees, in which linkage mapping is difficult, for cases with previously unrecognized or atypical phenotypes, and for disorders with high genetic heterogeneity [28,29]. Because congenital cataract shows wide phenotypic variability and genetic heterogeneity, WES is appropriate to reach a correct genetic diagnosis. In fact, we performed WES in three families showing congenital cataract and identified pathogenic mutations in two as described here, supporting that WES is quite powerful for dissecting the genetic basis of congenital cataract. Because the cost of WES is now falling, it is likely to be provided as a clinical service in the very near future and will provide useful information for genetic counseling and family planning in congenital cataract. In conclusion, WES successfully identified pathogenic mutations in two Korean families with congenital cataract, clearly demonstrating the efficiency and diagnostic utility of this technique in congenital cataract.

## APPENDIX 1.

Whole-exome sequencing performance. To access the data, click or select the words "Appendix 1."

## APPENDIX 2.

Candidate genes for congenital cataract. To access the data, click or select the words "Appendix 2."

## ACKNOWLEDGMENTS

We would like to thank the patients and their families for their participation in this study. This work was supported by research grants from the Ministry of Health, Labour and Welfare (H Saitsu, N Miyake, N Matsumoto) (12944231) and the Japan Science and Technology Agency (N Matsumoto) (11800122); a Grant-in-Aid for Scientific Research on Innovative Areas-(Transcription cycle)-from the Ministry of Education, Culture, Sports, Science and Technology of Japan (N Matsumoto) (12906972); a Grant-in-Aid for Scientific Research from the Japan Society for the Promotion of Science (N Matsumoto) (12940356); a Grant-in-Aid for Young Scientists from the Japan Society for the Promotion of Science (H Saitsu, N Miyake); and a grant from the Takeda Science Foundation (N Miyake and N Matsumoto).

## REFERENCES

- Rahi JS, Dezaux C. Measuring and interpreting the incidence of congenital ocular anomalies: lessons from a national study of congenital cataract in the UK. *Invest Ophthalmol Vis Sci* 2001; 42:1444-8. [PMID: 11381045].
- Chan WH, Biswas S, Ashworth JL, Lloyd IC. Congenital and infantile cataract: aetiology and management. *Eur J Pediatr* 2012; 171:625-30. [PMID: 22383071].
- Churchill A, Graw J. Clinical and experimental advances in congenital and paediatric cataracts. *Philos Trans R Soc Lond B Biol Sci* 2011; 366:1234-49. [PMID: 21402583].
- Bermejo E, Martinez-Frias ML. Congenital eye malformations: clinical-epidemiological analysis of 1,124,654 consecutive births in Spain. *Am J Med Genet* 1998; 75:497-504. [PMID: 9489793].
- Hejtmancik JF. Congenital cataracts and their molecular genetics. *Semin Cell Dev Biol* 2008; 19:134-49. [PMID: 18035564].
- Santhiya ST, Soker T, Klopp N, Illig T, Prakash MV, Selvaraj B, Gopinath PM, Graw J. Identification of a novel, putative cataract-causing allele in *CRYAA* (G98R) in an Indian family. *Mol Vis* 2006; 12:768-73. [PMID: 16862070].
- Hansen L, Yao W, Eiberg H, Kjaer KW, Baggesen K, Hejtmancik JF, Rosenberg T. Genetic heterogeneity in microcornea-ataract: five novel mutations in *CRYAA*, *CRYGD*, and *GJA8*. *Invest Ophthalmol Vis Sci* 2007; 48:3937-44. [PMID: 17724170].
- Huang B, He W. Molecular characteristics of inherited congenital cataracts. *Eur J Med Genet* 2010; 53:347-57. [PMID: 20624502].
- Weisschuh N, Aisenbrey S, Wissinger B, Riess A. Identification of a novel *CRYBB2* missense mutation causing congenital autosomal dominant cataract. *Mol Vis* 2012; 18:174-80. [PMID: 22312185].
- Bamshad MJ, Ng SB, Bigham AW, Tabor HK, Emond MJ, Nickerson DA, Shendure J. Exome sequencing as a tool for Mendelian disease gene discovery. *Nat Rev Genet* 2011; 12:745-55. [PMID: 21946919].
- Miyamoto T, Yu YS, Sato H, Hayashi H, Sakugawa N, Ishikawa M, Sengoku K. Mutational analysis of the human *MBX* gene in four Korean families demonstrating microphthalmia with congenital cataract. *Turk J Pediatr* 2007; 49:334-6. [PMID: 17990594].
- Li H, Ruan J, Durbin R. Mapping short DNA sequencing reads and calling variants using mapping quality scores. *Genome Res* 2008; 18:1851-8. [PMID: 18714091].
- Litt M, Kramer P, LaMorticella DM, Murphey W, Lovrien EW, Weleber RG. Autosomal dominant congenital cataract associated with a missense mutation in the human alpha crystallin gene *CRYAA*. *Hum Mol Genet* 1998; 7:471-4. [PMID: 9467006].
- Fu L, Liang JJ. Detection of protein-protein interactions among lens crystallins in a mammalian two-hybrid system assay. *J Biol Chem* 2002; 277:4255-60. [PMID: 11700327].
- Ghosh JG, Clark JI. Insights into the domains required for dimerization and assembly of human alphaB crystallin. *Protein Sci* 2005; 14:684-95. [PMID: 15722445].
- Ren Z, Li A, Shastry BS, Padma T, Ayyagari R, Scott MH, Parks MM, Kaiser-Kupfer MI, Hejtmancik JF. A 5-base insertion in the gammaC-crystallin gene is associated with autosomal dominant variable zonular pulverulent cataract. *Hum Genet* 2000; 106:531-7. [PMID: 10914683].
- Héon E, Priston M, Schorderet DF, Billingsley GD, Girard PO, Lubsen N, Munier FL. The gamma-crystallins and human cataracts: a puzzle made clearer. *Am J Hum Genet* 1999; 65:1261-7. [PMID: 10521291].
- Yao K, Jin C, Zhu N, Wang W, Wu R, Jiang J, Shentu X. A nonsense mutation in *CRYGC* associated with autosomal dominant congenital nuclear cataract in a Chinese family. *Mol Vis* 2008; 14:1272-6. [PMID: 18618005].
- Zhang L, Fu S, Ou Y, Zhao T, Su Y, Liu P. A novel nonsense mutation in *CRYGC* is associated with autosomal dominant congenital nuclear cataracts and microcornea. *Mol Vis* 2009; 15:276-82. [PMID: 19204787].
- Talla V, Narayanan C, Srinivasan N, Balasubramanian D. Mutation causing self-aggregation in human gammaC-crystallin leading to congenital cataract. *Invest Ophthalmol Vis Sci* 2006; 47:5212-7. [PMID: 17122105].
- Lindhurst MJ, Sapp JC, Teer JK, Johnston JJ, Finn EM, Peters K, Turner J, Cannons JL, Bick D, Blakemore L, Blumhorst C, Brockmann K, Calder P, Cherman N, Deardorff MA, Everman DB, Golas G, Greenstein RM, Kato BM, Keppler-Noreuil KM, Kuznetsov SA, Miyamoto RT, Newman K, Ng D, O'Brien K, Rothenberg S, Schwartztruber DJ, Singhal V, Tirabosco R, Upton J, Wientroub S, Zackai EH, Hoag K, Whitewood-Neal T, Robey PG, Schwartzberg PL, Darling TN, Tosi LL, Mullikin JC, Biesecker LG. A mosaic activating mutation in *AKT1* associated with the Proteus syndrome. *N Engl J Med* 2011; 365:611-9. [PMID: 21793738].

22. Lee JH, Huynh M, Silhavy JL, Kim S, Dixon-Salazar T, Heiberg A, Scott E, Bafna V, Hill KJ, Collazo A, Funari V, Russ C, Gabriel SB, Mathern GW, Gleeson JG. De novo somatic mutations in components of the PI3K-AKT3-mTOR pathway cause hemimegalencephaly. *Nat Genet* 2012; 44:941-5. [PMID: 22729223].
23. Lindhurst MJ, Parker VE, Payne F, Sapp JC, Rudge S, Harris J, Witkowski AM, Zhang Q, Groeneveld MP, Scott CE, Daly A, Huson SM, Tosi LL, Cunningham ML, Darling TN, Geer J, Gucev Z, Sutton VR, Tziotziou C, Dixon AK, Helliwell T, O'Rahilly S, Savage DB, Wakelam MJ, Barroso I, Biesecker LG, Semple RK. Mosaic overgrowth with fibroadipose hyperplasia is caused by somatic activating mutations in *PIK3CA*. *Nat Genet* 2012; 44:928-33. [PMID: 22729222].
24. Pagnamenta AT, Lise S, Harrison V, Stewart H, Jayawant S, Quaghebeur G, Deng AT, Murphy VE, Sadighi Akha E, Rimmer A, Mathieson I, Knight SJ, Kini U, Taylor JC, Keays DA. Exome sequencing can detect pathogenic mosaic mutations present at low allele frequencies. *J Hum Genet* 2012; 57:70-2. [PMID: 22129557].
25. Vissers LE, de Ligt J, Gilissen C, Janssen I, Steehouwer M, de Vries P, van Lier B, Arts P, Wieskamp N, del Rosario M, van Bon BW, Hoischen A, de Vries BB, Brunner HG, Veltman JA. A de novo paradigm for mental retardation. *Nat Genet* 2010; 42:1109-12. [PMID: 21076407].
26. Awadalla P, Gauthier J, Myers RA, Casals F, Hamdan FF, Griffing AR, Cote M, Henrion E, Spiegelman D, Tarabeux J, Piton A, Yang Y, Boyko A, Bustamante C, Xiong L, Rapoport JL, Addington AM, DeLisi JL, Krebs MO, Joobler R, Millet B, Fombonne E, Mottron L, Zilvermit M, Keebler J, Daoud H, Marineau C, Roy-Gagnon MH, Dube MP, Eyre-Walker A, Drapeau P, Stone EA, Lafreniere RG, Rouleau GA. Direct measure of the de novo mutation rate in autism and schizophrenia cohorts. *Am J Hum Genet* 2010; 87:316-24. [PMID: 20797689].
27. O'Roak BJ, Deriziotis P, Lee C, Vives L, Schwartz JJ, Girirajan S, Karakoc E, Mackenzie AP, Ng SB, Baker C, Rieder MJ, Nickerson DA, Bernier R, Fisher SE, Shendure J, Eichler EE. Exome sequencing in sporadic autism spectrum disorders identifies severe de novo mutations. *Nat Genet* 2011; 43:585-9. [PMID: 21572417].
28. Majewski J, Wang Z, Lopez I, Al Humaid S, Ren H, Racine J, Bazinet A, Mitchel G, Braverman N, Koeneke RK. A new ocular phenotype associated with an unexpected but known systemic disorder and mutation: novel use of genomic diagnostics and exome sequencing. *J Med Genet* 2011; 48:593-6. [PMID: 21862673].
29. Tsurusaki Y, Okamoto N, Suzuki Y, Doi H, Saito H, Miyake N, Matsumoto N. Exome sequencing of two patients in a family with atypical X-linked leukodystrophy. *Clin Genet* 2011; [PMID: 21644943].

Articles are provided courtesy of Emory University and the Zhongshan Ophthalmic Center, Sun Yat-sen University, P.R. China. The print version of this article was created on 18 February 2013. This reflects all typographical corrections and errata to the article through that date. Details of any changes may be found in the online version of the article.